



---

# Model Helicopter Rotor High-Speed Impulsive Noise: Measured Acoustics and Blade Pressures

---

D.A. Boxwell, F.H. Schmitz, W.R. Splettstoesser  
and K.J. Schultz

---

(NASA-TM-85850) MODEL HELICOPTER ROTOR HIGH-SPEED IMPULSIVE NOISE: MEASURED ACOUSTICS AND BLADE PRESSURES (NASA) 36 p HC A03/NF A01 CSCL 01A G3/02 42258  
n84-10020 Unclass

September 1983



---

# Model Helicopter Rotor High-Speed Impulsive Noise: Measured Acoustics and Blade Pressures

---

D. A. Boxwell,  
F. H. Schmitz, Aeromechanics Laboratory, Research and Technology Laboratories,  
U. S. Army Aviation Research and Development Command,  
Ames Research Center, Moffett Field, California

W. R. Spletstoesser,  
K. J. Schultz, DFVLR, Institut f. Entwurfsaerodynamik,  
Abt. Technische Akustik, Braunschweig, W. Germany

**NASA**

National Aeronautics and  
Space Administration

**Ames Research Center**  
Moffett Field California 94035

United States Army  
Aviation Research and  
Development Command  
St. Louis, Missouri 63166



MODEL HELICOPTER ROTOR HIGH-SPEED IMPULSIVE NOISE:  
MEASURED ACOUSTICS AND BLADE PRESSURES

D. A. Boxwell and F. H. Schmitz

Aeromechanics Laboratory  
U.S. Army Research and Technology Laboratories  
NASA Ames Research Center  
Moffett Field, California 94035 U.S.A.

W. R. Spletstoesser and K. J. Schultz

DFVLR, Institut f. Entwurfsaerodynamik  
Abt. Technische Akustik, Braunschweig, W. Germany

Abstract

A 1/7-scale research model of the AH-1 series helicopter main rotor was tested in the open-jet anechoic test section of the Deutsch-Niederlaendischer Windkanal (DNW) (Netherlands). Model-rotor acoustic and simultaneous blade pressure data were recorded at high forward speeds where full-scale helicopter high-speed impulsive noise levels are known to be dominant. Model-rotor measurements of the peak acoustic pressure levels, waveform shapes, and directivity patterns are directly compared with full-scale investigations, using an equivalent in-flight technique. Model acoustic data are shown to scale remarkably well in shape and in amplitude with full-scale results. Model rotor-blade pressures are presented for rotor operating conditions both with and without shock-like discontinuities in the radiated acoustic waveform. Acoustically, both model and full-scale measurements support current evidence that above certain high subsonic advancing-tip Mach numbers ( $M_{AT} \geq 0.9$ ), local shock waves that exist on the rotor blades "delocalize" and radiate to the acoustic far-field.

1. Introduction

Over the past few years, the understanding and prediction of high-speed impulsive noise of helicopter rotors have improved dramatically. Through fundamental experiments in an aerodynamically and acoustically controlled hover environment and through precise numerical computation, some of the important parameters of this annoying and detectable rotor noise have been isolated. These fundamental studies have shown that in addition to blade geometry, the local transonic flow field surrounding the transonic hovering rotor can be an important and vital contributor to the radiated noise (Refs. [1-3]). At locally transonic conditions, shocks near the tip of the finite-thick rotor blade can escape ("delocalize") to the acoustic far-field (Ref. [1]). The tip Mach number at which this phenomenon is observed is called the "delocalization Mach number" and is strongly affected by the local blade geometry in the tip region.

Although the hovering rotor is ideal for the fundamental study of transonic aerodynamics and noise, it does not exactly duplicate the flow environment of helicopter rotors which normally radiate high-speed impulsive noise. The primary reason is the large velocity asymmetry which exists on helicopters in high-speed forward flight. On the advancing side of the rotor, the rotor-blade rotational velocity sums with the helicopter's forward velocity, often causing advancing-tip speeds to approach Mach 1. On the retreating side of the rotor, the rotational velocity and forward velocity are in opposite directions yielding low effective velocities. As a result, the helicopter rotor blade sees a continually changing velocity field as it rotates through each revolution. On the advancing side of the rotor, where velocities are high, angles of attack are small; on the retreating side, the angles of attack are quite high because of low relative velocities. Therefore, in high-speed forward flight, rotor-blade dynamic stall on the retreating side of the rotor is a real possibility. To avoid this problem, the helicopter rotor-blade must not be too thin (0.06 to 0.12 c), a constraint that aggravates the advancing-blade transonic aerodynamic and high-speed noise problems. If advancing-tip Mach numbers are high, the relatively thick airfoils encounter large regions of unsteady transonic flow and delocalization occurs, allowing local shock waves on the airfoil surface to radiate to the acoustic far-field (Ref. [4]).

Acoustic prediction of the resulting noise for high-speed helicopter flight was attempted some years ago using linear models with limited success (Ref. [5]). As in the high-speed hover problem, nonlinear transonic aerodynamics play a significant role in the acoustic radiation and must be included in the modeling. However, the high-speed helicopter transonic flow field is unsteady. This further complicates the aerodynamic transonic flow-field computations by making far-field acoustic predictions of high-speed impulsive noise more difficult than the transonic-hover problem. To date, no computer code has successfully predicted the amplitude or waveform of high-speed impulsive noise in forward flight when shock waves delocalize to the acoustic far-field.

An alternative to the analytical approach is to duplicate the full-scale high-speed impulsive noise in model scale. Although this procedure seems straightforward, most previous acoustic full-scale, ground-based, and wind-tunnel testing required data corrections that made quantitative comparisons quite difficult. Early model-to-full-scale comparisons on a hovering rotor were encouraging but qualitative (Ref. [6]). More recent model-scale wind-tunnel comparisons with ground-based, full-scale measurements (Ref. [7]) showed general agreement after the data were corrected for microphone position differences, reverberation, atmospheric and ground attenuation, and forward velocity effects (Doppler shift).

Many of these data corrections are not necessary if the full-scale data are gathered by using the in-flight technique developed by the Aeromechanics Laboratory (Ref. [8]). The technique consists of mounting microphones on a quiet, fixed-wing aircraft that is flown in formation with the subject helicopter over a matrix of flight conditions. Because relative geometry between the measurement aircraft

and subject helicopter is essentially fixed, the procedure is equivalent to wind-tunnel testing. In full-scale flight, the microphone and subject helicopter maintain the same relative locations while flying through air at the same flight conditions. In wind-tunnel testing, the in-flow microphones and the rotor in a uniform air flow are fixed in space at similar relative positions. Aerodynamically and acoustically the procedures are the same, provided that the background noise and acoustic reflections of both in-flight and wind-tunnel testing are minimized.

The in-flight procedure was used to gather acoustic data over a fairly complete matrix of flight conditions for the UH-1H helicopter (Ref. [8]). Because this was really the first series of tests with the in-flight, far-field measuring technique, some acoustic data scatter was evident. These data were first compared with 1/7-scale model UH-1H acoustic data gathered in an acoustically treated, hard-walled wind tunnel (Ref. [4]). Although tunnel reverberation effects did influence the results of the model-scale data at lower advancing-tip Mach numbers, reasonably good quantitative model-scale to full-scale correlation was achieved. Certainly, many of the full-scale temporal shapes and amplitude trends were duplicated in the model-scale experiment.

Another attempt at model-to-full-scale rotor acoustic scaling was made with the AH-1 series helicopter. Carefully controlled performance and in-flight acoustic tests (Refs. [9] and [10]) were run on a standard AH-1/540 rotor over a full matrix of flight conditions and compared with a 1/7-scale model operational-loads-survey (OLS) rotor tested under similar conditions in a 3-m (9.8-ft) open-jet, anechoic wind tunnel, CEPR-19 (Ref. [11]). Although the blade-vortex interaction impulsive noise phenomenon was shown to scale fairly well, wind-tunnel speed constraints did not allow the high-speed impulsive noise scaling question to be fully addressed.

This same OLS model rotor was recently tested in the acoustically treated DNW over a full range of testing conditions, some of which are reported here. The emphasis in this paper is on carefully exploring the important scaling parameters of helicopter-rotor, high-speed impulsive noise. In addition, the directivity of the radiating noise field is documented along with selected blade pressures at several high subsonic advancing-tip Mach numbers.

## 2. Experimental Design

The model-rotor test was performed in the new German-Dutch wind tunnel, Deutsch-Niederländischer Windkanal (DNW), which is located about 150 km northeast of Amsterdam, the Netherlands; an aerial view of this facility is shown in Fig. 1. (The testing and subsequent data reduction efforts are part of a continuing memorandum of understanding for cooperative research between the German and United States governments.) The DNW is a subsonic, atmospheric wind tunnel of the closed-return type; it has three interchangeable, closed, test-section configurations and one open-jet configuration with a 6- by 8-m (19.7- by 26.2-ft) contraction. The tunnel was designed for low background

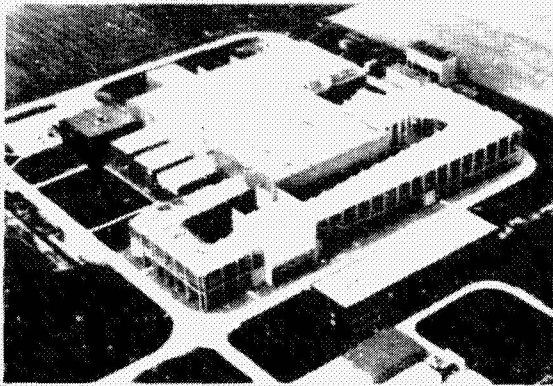


Fig. 1. Aerial view of the German-Dutch wind tunnel, DNW.

ties with low unsteady disturbances over the total testing velocity range. The more important tunnel characteristics for rotor aero/acoustic testing are given in Appendix A of Ref. [12]. (Additional DNW information can be found in Ref. [13].) The open-jet configuration with the 6- by 8-m (19.7- by 26.2-ft) contraction was used for the rotor tests reported here, the test rig being placed 7 m (23 ft) downstream of the nozzle at the normal model location in the center of the 20-m (65.6-ft) long free jet. The maximum wind velocity in this configuration is 85 m/sec ( $\approx 165$  knots), which covers the full speed range of modern helicopters.

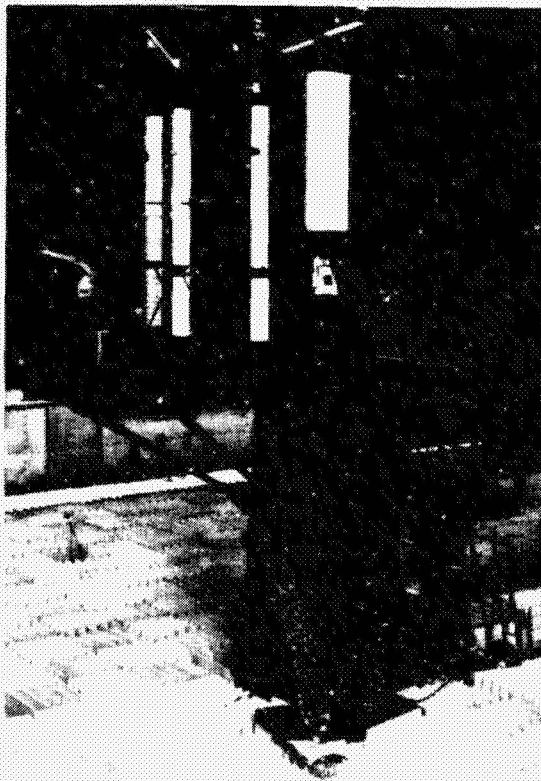


Fig. 2. Rotor test stand mounted in the DNW open test section.

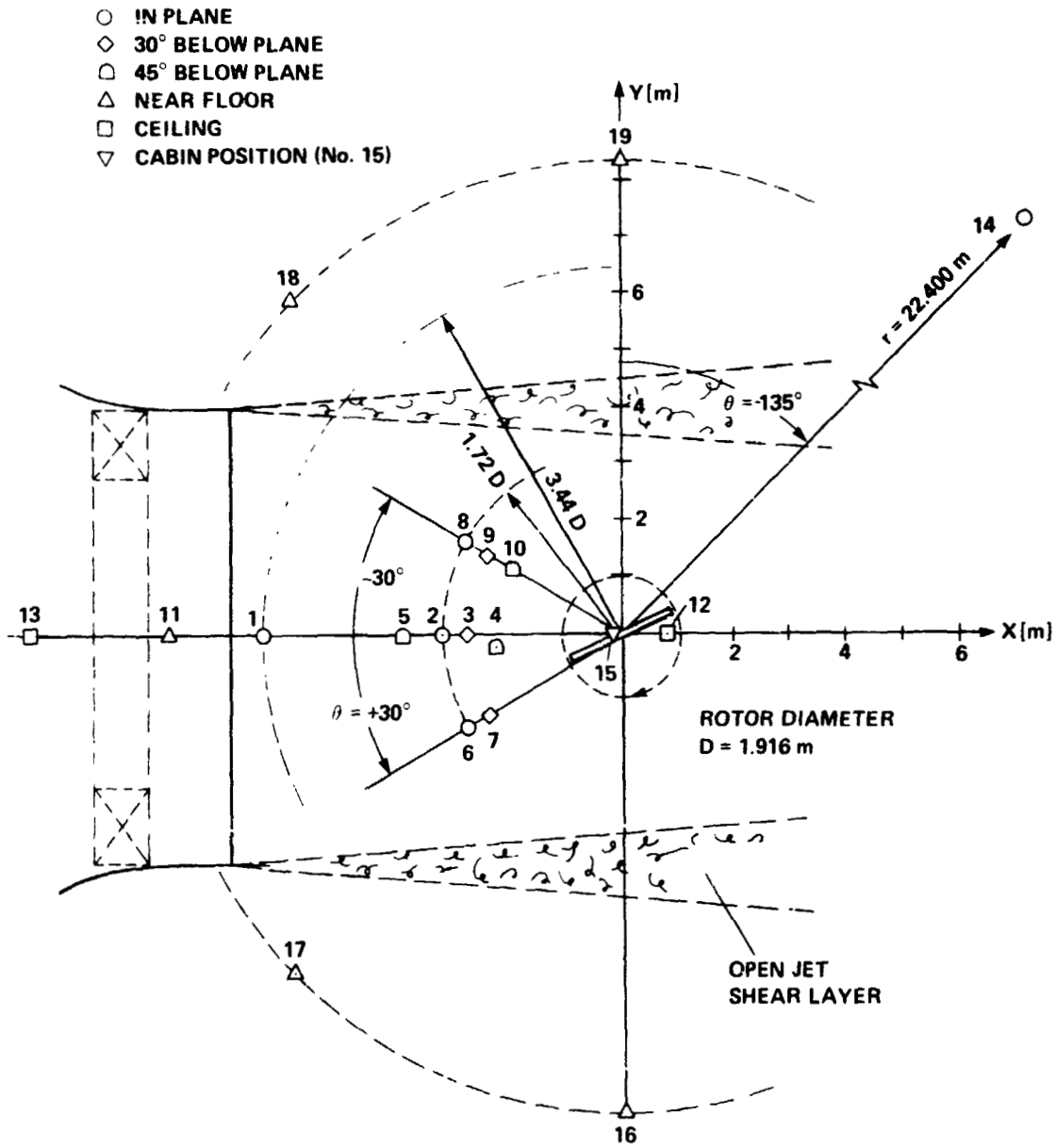
noise by choosing a low-tip-speed fan and by acoustically lining the turning vanes and collector/transition walls. An acoustically treated testing hall of more than  $30,000 \text{ m}^3$  ( $1.06 \times 10^6 \text{ ft}^3$ ) surrounds the open-jet testing configuration, most of which is usable for in-flow or out-of-flow acoustic measurements. The resulting good anechoic properties (cutoff frequency of 80 Hz) makes the DNW the free world's largest aeroacoustic wind tunnel. The tunnel also has excellent fluid dynamic quali-

The model-rotor and microphone installation in the open test-section of the DNW is shown in Fig. 2. The Aero-mechanics Laboratory's rotor test stand was mounted on a specially fabricated tower designed and constructed by DNW and DFVLR personnel. This structure placed the rotor on the tunnel centerline, 10 m (32.8 ft) above the testing hall floor. The in-flow microphones were supported by streamlined struts which were also attached to the tower structure. As shown in Fig. 2, the rotor test stand was shrouded with an aerodynamic fairing and wrapped with 25 mm (1 in.) of acoustic, open-celled foam to reduce sound reflections. An open-celled textile material (hospital bandage) was then wrapped around the foam to permanently secure it to the fairing. The same technique

was used on the three main-microphone support struts located within the free jet. In the initial stages of testing, foam treatment of the microphone supports was not thought to be necessary. However, on-line acoustic calibration of the test configuration showed reflections from the support struts, which would have distorted the measured rotor acoustic signals (see Appendix B of Ref. [12]). Additional acoustic calibrations with and without flow yielded the final test configuration shown in Fig. 2.

A total of 19 B&K 1/4-in. microphones (Type 4135) were distributed around the rotor, 10 in the open-jet core flow and 9 out of it (Fig. 3). The location of the in-flow microphones, typically 3.26 m (10.7 ft) from the rotor hub, was chosen to correspond to an average scaled microphone position of the full-scale acoustic tests of Refs. [9] and [10]. All of the in-flow microphones (Nos. 1-4, 6-10, and 15) were positioned forward and down from the rotor-hub plane, where severe impulsive noise is known to radiate (Ref. [8]). Another in-flow microphone (No. 1) was placed in-plane directly in front of the nozzle lip at exactly twice the distance (6.52 m (21.4 ft)). In-plane forward flight acoustic decay rates were measured by comparing acoustic levels from microphones Nos. 1 (6.52 m) and 2 (3.26 m). One additional microphone (No. 15) was placed in the flow underneath the rotor in the model-scaled cabin position to measure impulsive noise that would be heard in the cabin. The in-flow microphones were carefully foam-bedded in special adapters and equipped with nose cones pointing upstream into the oncoming flow. The out-of-flow microphones - most of which were located near the floor (Nos. 5, 11, 16-19), above the rotor plane (Nos. 12 and 13), and toward the aft quadrant (No. 14) of the rotor - were used to gather additional information about directivity, distance, and shear-layer effects. They were equipped with standard grid and wind screens and oriented for grazing incidence. Microphone calibrations were accomplished with B&K piston-phones on the beginning or end of each recorded magnetic tape. For intermediate checks, the insert voltage method was applied. Although not an absolute calibration method (because the diaphragm sensitivity is not included in the calibration procedure), insert voltage can be easily applied as an electrical checkout of the microphone circuit. The importance of having "simple" acoustic "checks" in a large testing facility, such as the DNW, should be emphasized. These procedures helped to assure the validity of the recorded data and thereby minimize unproductive test time. In addition, calibration data for the blade-pressure transducers were recorded at 0 and 2.76 N/cm<sup>2</sup> (0 and 4 lb/in.<sup>2</sup>) static pressure. This was done simultaneously for all transducers by placing the blade within a portable plastic cylindrical sleeve and evacuating it to the desired calibration pressure.

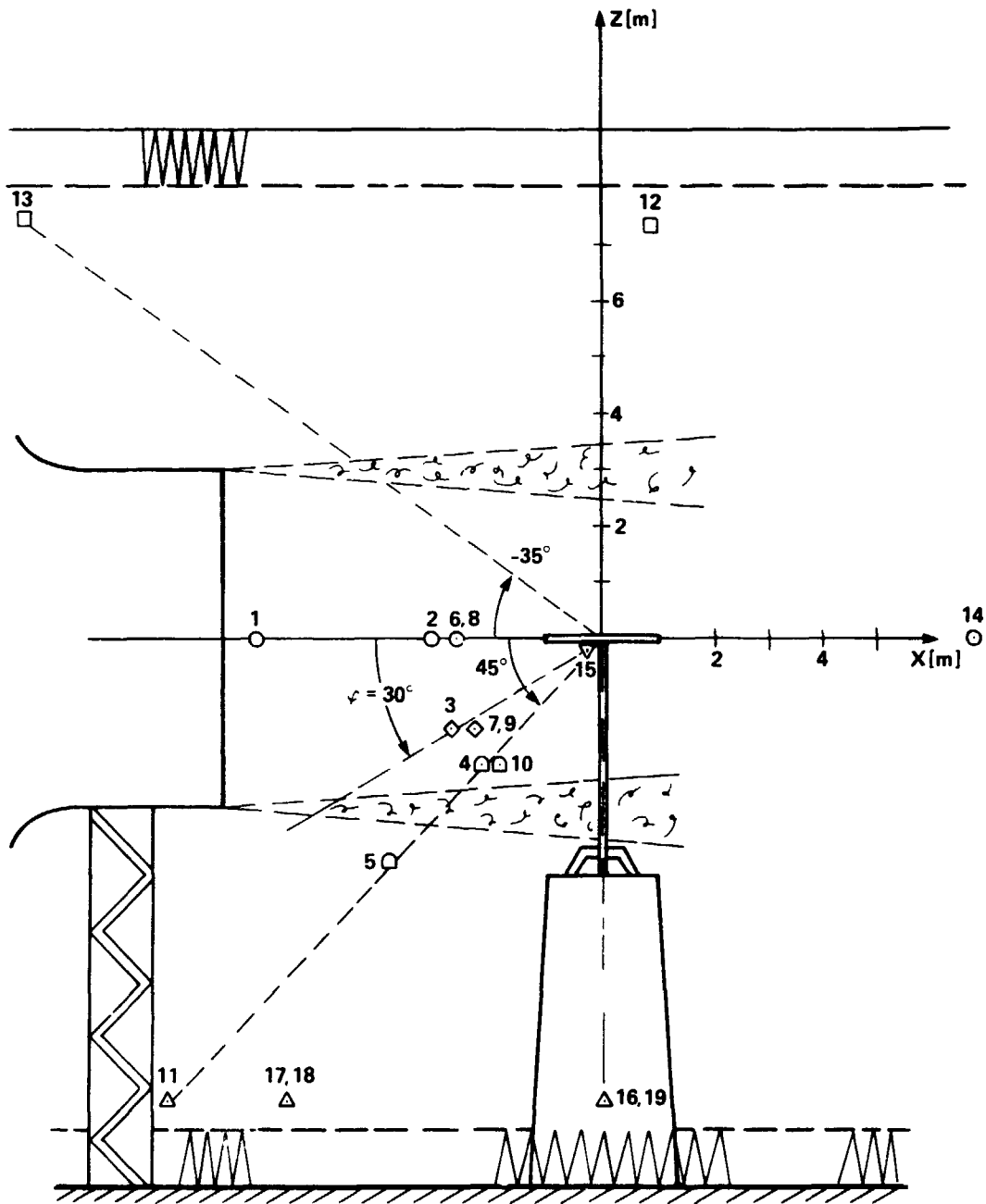
The model-rotor blades were mounted on a teetering-hub assembly, with the collective and the longitudinal and lateral cyclic rotor inputs provided by remotely controlled electric swashplate actuators. Tip-path-plane tilt was controlled directly through cyclic, the shaft being rigidly mounted in the vertical position on the rotor stand. A six-component strain-gauge balance, comprising the top portion of the rotor stand, was used to monitor and record rotor thrust, drag, and pitching moments for each test condition. Blade-surface pressures, blade flapping, and tunnel temperature were all measured in the



(a) Top view.

Fig. 3. Microphone locations in the DNW.

ORIGINAL PAGE IS  
OF POOR QUALITY



(b) Side view.

Fig. 3. Concluded.

rotating-hub frame; measurement data were transmitted by wires to the lower end of the shaft, and transferred to a nonrotating frame via a 156-channel slip-ring assembly. Rotor-shaft rotational encoders of 1/rev, 60/rev, and 180/rev were used to accurately control rpm and to azimuthally index rotor events. An automatic servo system was used to control a variable-frequency, 90-hp electric motor that drove the model rotor up to 3,000 rpm. For all test cases, the ambient drive system noise was below the wind-noise floor, with practically no effect on the rotor noise measurements (see Appendix B of Ref. [12]). All the microphone signals and selected pressure data were monitored on-line and, after proper signal conditioning, simultaneously recorded on three multichannel, FM, magnetic tape recorders with a total of 60 channels set for a recording speed of 76.2 cm/sec (30 ips) and a frequency response of 20 kHz. Flapping potentiometer output, balance data, and also the outputs from a hot-wire probe placed near microphone No. 6, and from one accelerometer positioned in the blade near the tip were recorded along with the acoustic and pressure data. IRIG-B time-code and rotor azimuth signals were recorded on each tape for synchronization purposes. During the 1-min data recording, two HP 5420A FFT analyzers were used to generate on-line instantaneous and averaged time-histories of selected microphones and pressure transducers. Wind-tunnel velocity, temperature, and dew point, as well as rotor speed, swashplate control inputs, and balance information, were processed on-line, using a portable HP 85 computer directly connected to the rotor balance.

### 3. Model-Rotor Characteristics

One of the main purposes of the test program was to quantitatively establish the validity of using scaled model-rotors to duplicate full-scale acoustic test results. Therefore, the in-flight data-gathering technique was used to obtain high-quality, stationary, full-scale data on the AH-1 series helicopter (Cobra) with the BHT 540 rotor blades. These data, gathered and reduced by the Aeromechanics Laboratory with the assistance of the Army Aviation Engineering Flight Activity, Edwards Air Force Base, and NASA Ames Research Center, is presented in detail in Refs. [9] and [10]. More recently, Ames Research Center has run a second series of in-flight acoustic tests on an AH-1G helicopter equipped with OLS rotor blades (Ref. [14]). The thickness and chord of the 540 rotor blade were increased slightly to accommodate many blade-surface pressure transducers. It is hoped that future investigations of rotor scaling will make use of these full-scale simultaneous blade-surface and far-field acoustic data.

A photograph of the two-bladed, teetering, 1/7 geometrically scaled AH-1/OLS model rotor is shown in Fig. 4. The rotor was instrumented with 50 miniature pressure transducers: 32 absolute flush-mounted Kulite transducers on one of the blades and 18 differential-pressure transducers on the second blade. The absolute transducer locations were chosen to match some of the radial and chordwise transducer positions in the full-scale tests of Ref. [14]. The geometric characteristics of the 1.916-m-diam (6.3-ft) model-scale OLS blades are shown in Fig. 5(a), and the absolute transducer locations are shown in Fig. 5(b). Some high-advancing-tip Mach number absolute

ORIGINAL PAGE IS  
OF POOR QUALITY

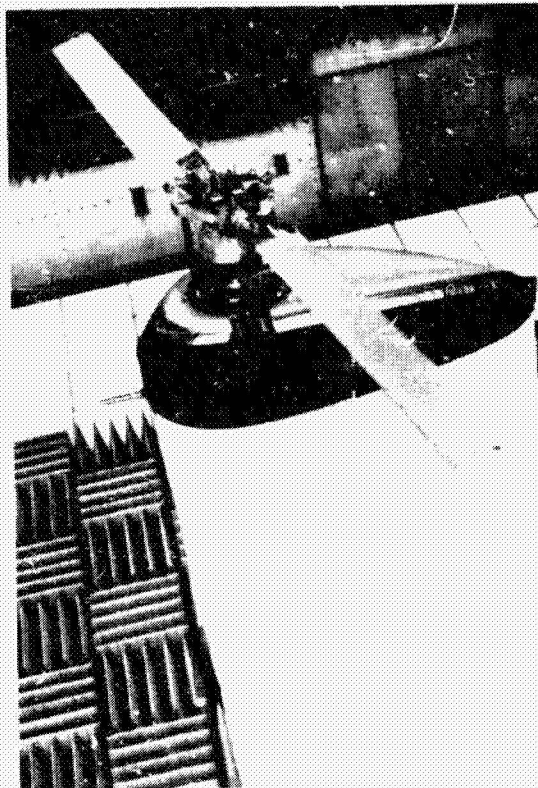
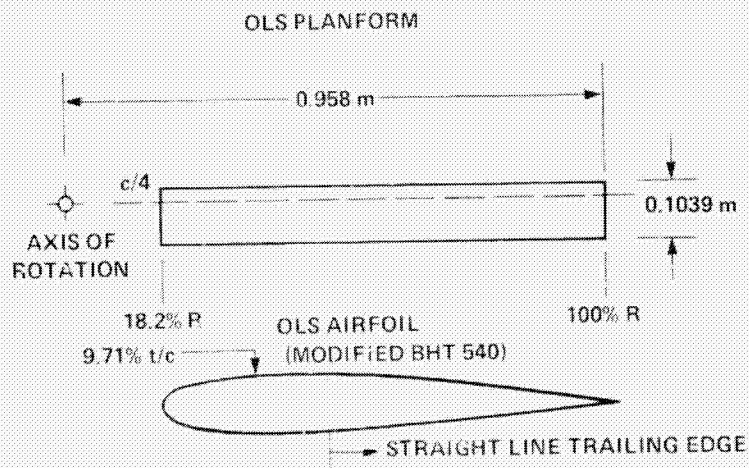
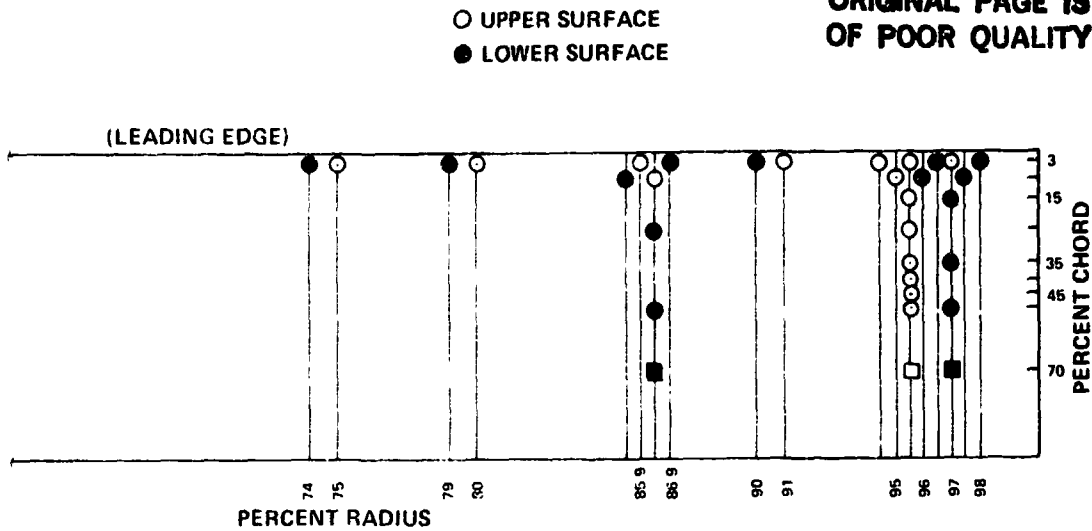


Fig. 4. Two-bladed OLS model rotor mounted on a teetering hub in the DNW.



(a) OLS blade geometry.

Fig. 5. Model AH-1/OLS rotor characteristics.



(b) Scale model AH-1/OLS rotor-blade absolute pressure transducer locations.

Fig. 5. Concluded.

blade pressure data are discussed in this paper. The rotor model is directly scaled from the full-scale OLS blades. As in the full-scale OLS blade, model-blade thickness and chord have been increased slightly over those of the standard BHT 540 AH-1 blade. Although the geometrical differences between the 540 and the OLS blades are small, they have been accounted for in the comparisons of the model OLS blade and the full-scale 540 blade acoustic measurements shown in this paper.

#### 4. Acoustic Scaling Parameters

Acoustic scaling, like most procedures that are dependent on fluid dynamic processes, is governed by the fundamental laws of mass and momentum. When the governing equations are placed in nondimensional form and the important nondimensional parameters of noise radiation are matched, it is possible to duplicate a large-scale acoustic event in small scale. A concise mathematical form (an integral equation) for the sound generated by bodies in arbitrary motion is given in Ref. [15]. In the Appendix of this paper, this equation is rewritten in nondimensional form (Eq. (A2)) and the results interpreted for model- and full-scale rotor testing.

One of the first conditions for model-to-full-scale acoustic scaling is geometric similarity. Thus, all model dimensions are  $1/\gamma$  times the full-scale dimensions of the noise generating surfaces:

$$\gamma = \frac{\text{full-scale length}}{\text{model-scale length}}$$

A second condition specified by Eq. (A2) is that the model and full-scale hover tip Mach numbers ( $M_H$ ) be identical. Thus, a geometrical reduction to model-scale by the scale factor  $\gamma$  must be offset by an increase of rotor-shaft rotational speed. Speed-of-sound differences between model and full-scale conditions must be accounted for. Therefore, the model-rotor shaft rotational speed  $\Omega_m$  (subscript m for model) is related to the full-scale shaft rotational speed by Eq. (A3):

$$\Omega_m = \gamma \frac{a_o}{a_{o_m}} \Omega$$

Also, a unit of model-scale time is related to full-scale time by Eq. (A4):

$$t_m = \frac{1}{\gamma} \frac{a_o}{a_{o_m}} t$$

All temporal data shown in this paper have been normalized by a rotor revolution or fraction thereof, thereby accounting for time-scaling differences.

As discussed in the Appendix, four nondimensional parameters have to be matched if model scale is to duplicate the full-scale phenomenon of interest. In addition to hover tip Mach number ( $M_H$ ) which was discussed above, they are advance ratio  $\mu$ , thrust coefficient  $C_T$ , and tip-path-plane angle  $\alpha_{TPP}$ . Of course, by matching full-scale hover tip Mach number and advance ratio, the advancing-tip Mach number ( $M_{AT}$ ) is automatically duplicated. For high-speed impulsive noise, advancing-tip Mach number instead of advance ratio is often chosen as the dominant nondimensional parameter. It controls, for the most part, how acoustic waves are radiated to the far-field (Ref. [4]).

If all of the governing nondimensional parameters of high-speed impulsive noise are matched, Eq. (A2) states that the acoustic pressure coefficient  $[C_p'(\bar{x}, \bar{t})]$  of the full-scale rotor is the same as the acoustic pressure coefficient of the model scale rotor  $[C_{p_m}'(\bar{x}_m, \bar{t}_m)]$ ; that is,

$$C_p'(\bar{x}, \bar{t}) = \frac{P'(\bar{x}, \bar{t})}{\rho_o a_o^2} = \frac{P_m'(\bar{x}_m, \bar{t}_m)}{\rho_{o_m} a_{o_m}^2} = C_{p_m}'(\bar{x}_m, \bar{t}_m) \quad (1)$$

If, as is normally the case, it is desired to compare dimensional pressure time-histories from two separate tests, where all the governing nondimensional parameters have been matched, it is necessary to adjust the pressure levels to account for differences in  $\rho_o a_o^2$ , which is proportional to the ambient pressure  $P_o$ . For convenience and in concert with past wind-tunnel acoustic practices, all acoustic data presented in this report will be referred to ISA standard day, sea-level pressure (indicated by \*). Thus, model-scale pressures measured during wind-tunnel testing become

ORIGINAL PAGE IS  
OF POOR QUALITY

ORIGINAL PAGE IS  
OF POOR QUALITY

$$P_m'^*(\bar{x}_m, \bar{t}_m) = \frac{P_m'(\bar{x}_m, \bar{t}_m)}{\rho_{O_m} a_{O_m}^2 / \rho_O^* a_O^{*2}}$$

or, in terms of ambient pressure ratio,

$$P_m'^*(\bar{x}_m, \bar{t}_m) = \frac{P_m'(\bar{x}_m, \bar{t}_m)}{\rho_{O_m} / \rho_O^*} \quad (2)$$

Because the DNW is located near sea level and normal operating conditions were always close to the ISA standard day, only small pressure ratio corrections  $P_{O_m}/P_O^*$  were necessary for the model acoustic data presented in this paper.

Similar correction procedures are necessary for flight-test data. Again, all acoustic data are referred to ISA standard day, sea-level pressure by

$$P'^*(\bar{x}, \bar{t}) = \frac{P'(\bar{x}, \bar{t})}{\rho_O a_O^2 / \rho_O^* a_O^{*2}} = \frac{P'(\bar{x}, \bar{t})}{P_O / P_O^*} \quad (3)$$

Because acoustic data were gathered at varying pressure altitudes, corrections were not insignificant for flight test data ( $P_O/P_O^*$  of the order 0.7 to 0.8).

This was really the first time that such procedures had been applied to rotor acoustic testing. Previously it was thought (Refs. [4] and [6-11]) that simply adjusting the measured pressures for density ratio (i.e.,  $\rho_O/\rho_O^*$ ) was adequate to correct pressures to sea-level standard conditions. However, the formal transformation of the governing equation to nondimensional form (presented in the Appendix) has shown this to be only partially correct. The complete adjustment requires corrections according to the ambient pressure ratio or equivalent to density and temperature ratio (since  $\rho_O a_O^2 / \rho_O^* a_O^{*2} = \rho_O T_O / \rho_O^* T_O^*$ ).

The model-rotor test program in the DNW comprised 3 wk of tunnel occupancy. Because this was the first rotor acoustic test in the free-jet of the DNW, 2 of the 3 wk were used for setup and in-place preoperational checkout. This calibration and checkout phase consisted of detection and attenuation of acoustic impulse reflections from the microphone support struts, background noise measurements, and a high-speed hovering check with untwisted UH-1H blades. This last check allowed the high-speed data taken in this facility to be compared with data from other acoustic facilities throughout the world (e.g., Ref. [16]). Some results and details of these calibration procedures are presented in Appendix B of Ref. [12]. In general, the DNW was shown to have some of the best rotor acoustic measurement capabilities in the world. In the remaining week of tunnel occupancy, a total of about 150 data points were taken, covering both blade-vortex-interaction and high-speed impulsive noise operating conditions. The range of the four governing nondimensional

parameters (hover tip Mach number  $M_H$ , advance ratio  $\mu$ , thrust coefficient  $C_T$ , and tip-path-plane angle  $\alpha_{TPP}$ ) covered were

$$\left. \begin{array}{l} M_H (0.55-0.72) \\ \mu (0.1-0.35) \end{array} \right\} M_{AT} (0.73-0.94)$$

$$C_T (0.0047-0.0065)$$

$$\alpha_{TPP} (-5^\circ - +7^\circ)$$

ORIGINAL PAGE IS  
OF POOR QUALITY

The nondimensional testing envelope of model-scale test conditions is shown in Fig. 6. Also presented in Fig. 6 are the dimensional rate-of-climb profiles of a simple performance model for the AH-1 helicopter (Cobra). The model-test data presented in this paper emphasize high-speed impulsive noise and thus encompass many test points in the right half of the cross-hatched region. For two reasons, many of these points were chosen to be representative of descending flight: (1) the full-scale data are, at times, gathered in descending flight because of power limitations of the YO-3A aircraft; and (2) a model-shaft-tilting capability was not available during the test, restricting the forward tip-path-plane ( $-\alpha_{TPP}$ ) angles at high forward speeds.

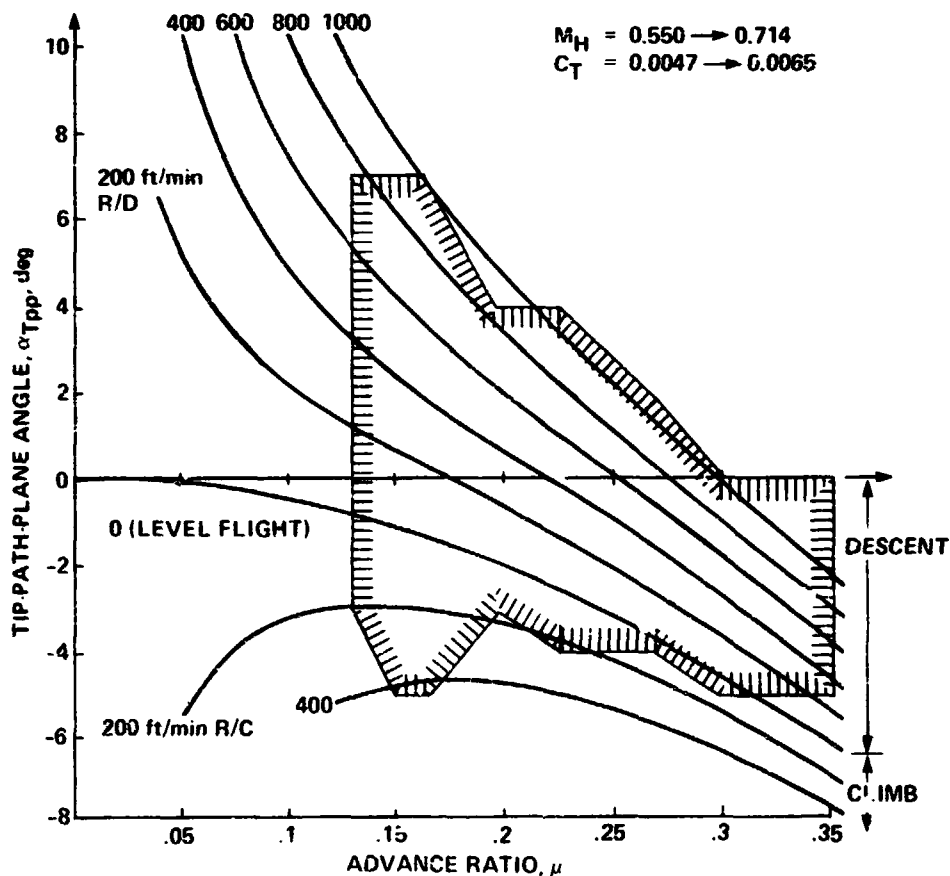


Fig. 6. OLS model testing envelope.

## 5. Model-Scale/Full-Scale Acoustic Comparisons

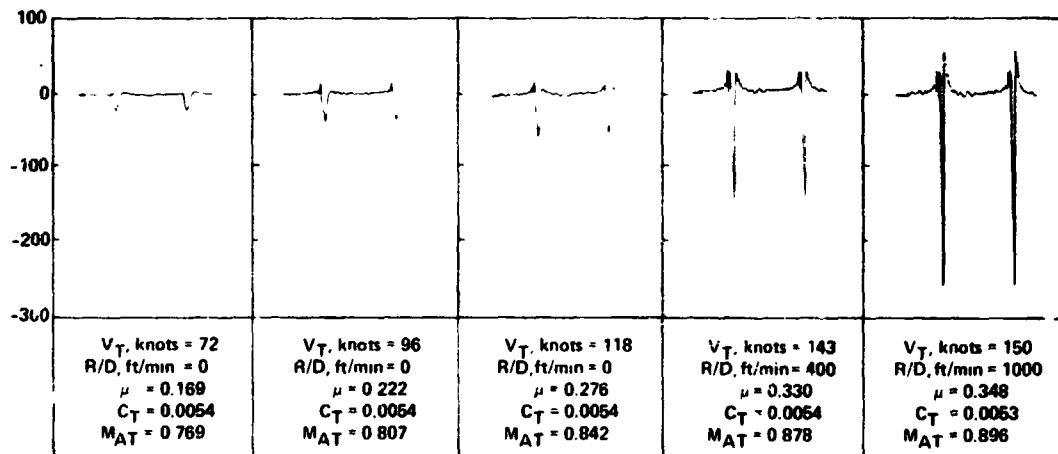
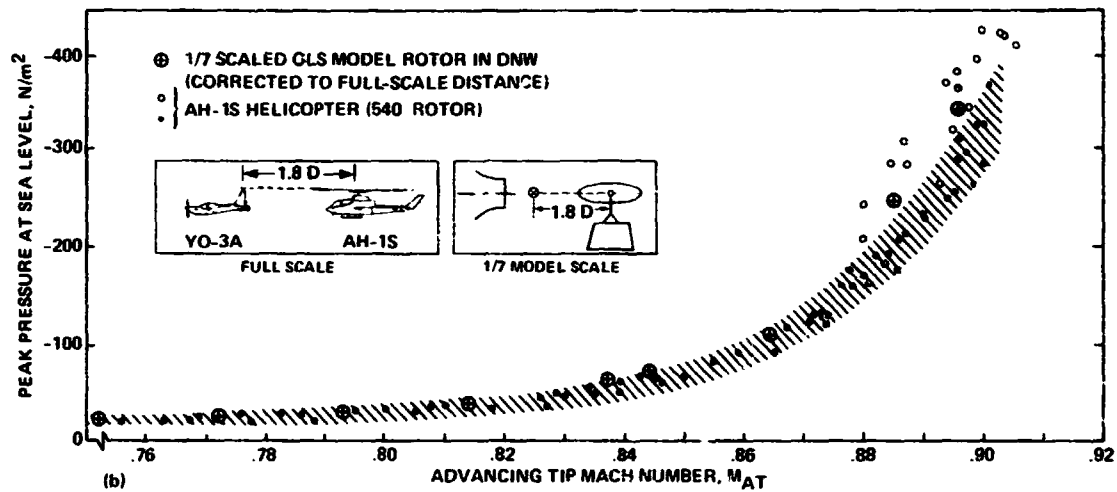
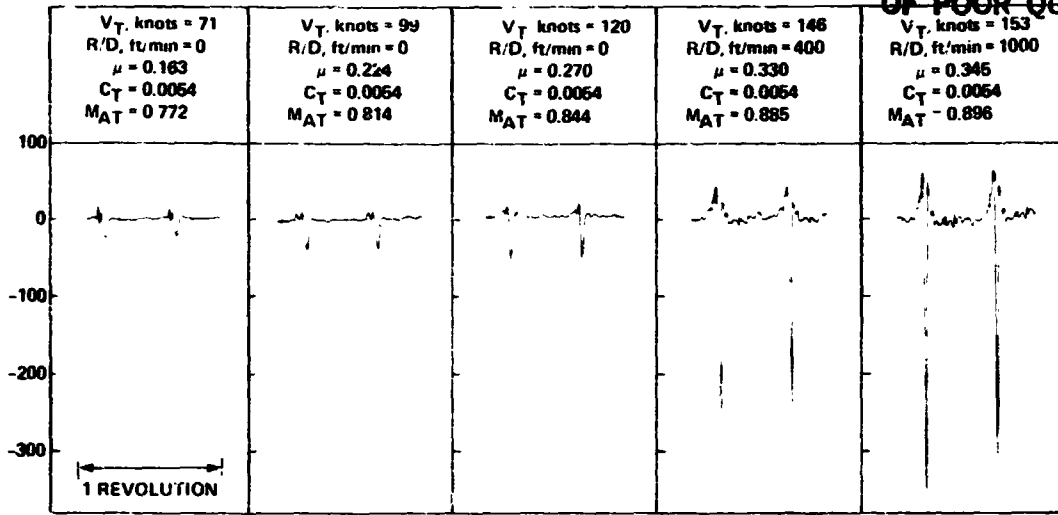
The simple and most direct method of comparing model-scale and full-scale acoustic data is through a detailed analysis of acoustic pressure time-histories. Such a comparison of AH-1/OLS model acoustic data with AH-1 full-scale data measured with the in-flight method developed and performed by Boxwell and Schmitz (Refs. [9] and [10]) is illustrated in Figs. 7 and 8. Negative peak pressure levels are plotted as a function of advancing-tip Mach number, the most important nondimensional parameter of high-speed impulsive noise. The sketches in Fig. 7(b) illustrate the equivalence of wind-tunnel and in-flight acoustic testing and indicate that the data shown were gathered by an in-plane microphone located 1.8 rotor diameters ahead of the hub. Because this is one of the easiest station-keeping positions for the in-flight data gathering method, the full-scale data shown are thought to be of high quality. All of the individual high-speed in-plane data points are shown in Fig. 7(b) (small circles and dots), illustrating a representative scatter band for the full-scale technique. The data indicated by circles were correlated with advancing-tip Mach number from the more unsteady runs. For these cases, the pilot made substantial adjustments to the collective control to hold current relative spatial position between the microphones mounted on the fixed-wing aircraft and the helicopter. These collective changes altered the rotor rpm, thereby changing the instantaneous advancing-tip Mach number. These effects were accounted for in the data shown by correlating the instantaneous acoustic pressures with instantaneous advancing-tip Mach number. The dots represent the more steady full-scale data points. For ease of comparison, they are generally indicated by the shaded area. The model-scale wind-tunnel data are shown by the circled crosses. In Fig. 7, the model acoustic data have been adjusted for the small differences in noise path lengths (using a  $1/r$  decay law which is discussed later) and blade thickness. The full-scale data have been corrected to ISA standard day sea-level pressure according to Eq. (3) in the previous section of this paper.

The model-scale/full-scale comparison of in-plane microphone data is excellent. Peak negative pressures and waveform shapes agree remarkably well over the entire Mach-number range tested.

Some small amplitude discrepancies are noted at the higher advancing-tip Mach numbers if the model scale data are compared with only the more steady full-scale data. Although there is no conclusive evidence to account for these small discrepancies, the difference between full-scale and model-scale blade/hub dynamic characteristics is thought to play a role. In particular, some preliminary calculations, performed by J. Corrigan of Bell Helicopter, indicate that simple lead-lag motion differences resulting from trim changes could account for full-scale advancing-tip Mach number reductions of 0.006. Although reductions in advancing-tip Mach number of 0.006 would be barely noticeable at low forward velocities, the effect could easily explain the small differences between model- and full-scale acoustic data shown at the high-advancing-tip Mach numbers.

OLS MODEL ROTOR ACOUSTIC SIGNATURES

ORIGINAL PAGE IS  
OF POOR QUALITY



(c) AH 1S (540 ROTOR) ACOUSTIC SIGNATURES

Fig. 7. Comparison of model and full-scale acoustic pressure for an in-plane microphone 1.8 rotor diameters ahead. (a) Model-scale results for one rotor revolution; (b) wind-tunnel and in-flight acoustic testing equivalence; (c) full-scale pressure-time histories for one rotor revolution.

The importance of this effect was also demonstrated during model testing in the DNW. After running at a condition of high-advancing-tip Mach numbers and high thrust, the feathering bearings became worn, allowing additional lead-lag blade motions of  $\pm 0.5^\circ$ . Acoustic data gathered under these conditions were reduced in amplitude by an average of 20% from those of a similar run taken with a good feathering bearing. It would appear that in-plane dynamics can play a significant role in the correlation between model and full-scale data. Fortunately, in the test reported here, the model and full-scale blades are stiff and heavy, thus minimizing these effects. However, for more modern rotors, which are more likely to be softer and lighter than the 540 rotor, the first mode of lead-lag, torsion, and flapping should probably be dynamically scaled.

The dramatic increase in peak pressure levels and the waveform shape changes that occur near the delocalization advancing-tip Mach number are illustrated in the averaged time-history inserts of Fig. 7; Fig. 7(a) shows the model-scale results and Fig. 7(c) the full-scale pressure-time histories for one rotor revolution. A definite change in pulse shape occurs in both the model-scale and full-scale data in the 0.86 to 0.9 advancing-tip Mach number range.

These changing waveform characteristics are more clearly indicated in Fig. 9 where the time-scale of one impulse has been lengthened. At advancing-tip Mach numbers of 0.864 and below, the high-speed impulsive noise waveform is almost symmetrical on both the model-scale and full-scale data. At slightly higher advancing-tip Mach numbers ( $M_{AT} \approx 0.885$ ), the waveform of the model-scale and full-scale data begin to change, becoming more saw-toothed. At advancing-tip Mach numbers near 0.9, the waveform has changed to a pronounced saw-toothed shape; that is, a large negative pressure peak is followed by a steep rise in pressure (shock). In effect, the local transonic fields of both the model-scale and full-scale have delocalized. A strong discontinuous pressure jump (shock) radiates uninterrupted from the unsteady transonic flow field surrounding each rotor-blade tip to the acoustic far-field (Refs. [1], [4], and [8]). The excellent correlation in waveform character in the delocalization advancing-tip Mach number region is a further demonstration of the excellent scaling between model-scale and full-scale high-speed impulsive noise data.

It should be noted that the full-scale acoustic data presented in this paper have been averaged to improve the signal/noise level and more completely define the character of the full-scale high-speed noise waveform. This was accomplished by signal-analysis techniques that utilize the dominant negative-pressure peaks to control the digitizing process instead of utilizing the 1/rev signals from the helicopter. Because the tail-rotor rotational frequency is a non-integer multiple of that of the main rotor, most tail-rotor noise is averaged out, leaving only the main-rotor impulsive noise signature for comparison purposes.

Some differences in the model-scale to full-scale pulse shapes do exist; they occur slightly before the large negative high-speed impulsive noise impulse, as illustrated in Fig. 8. These smaller

ORIGINAL PAGE IS  
OF POOR QUALITY

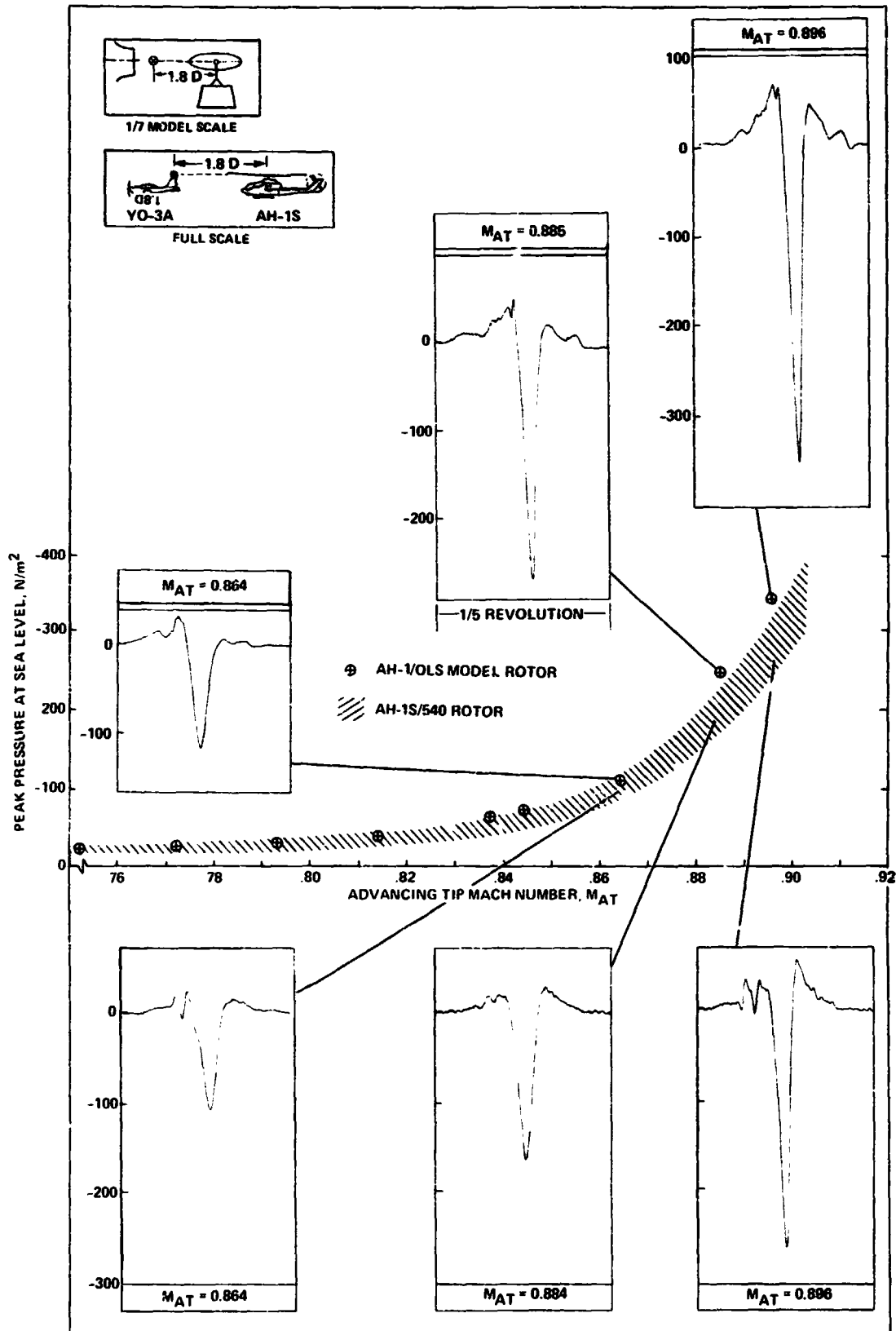


Fig. 8. Comparison of model and full-scale acoustic waveforms for an in-plane microphone 1.8 rotor diameters ahead.

ORIGINAL PAGE IS  
OF POOR QUALITY

differences in waveform shape are known to be strongly influenced by blade-vortex interactions (Ref. [11]). Small changes or differences between model- and full-scale tip-path-plane angles are thought to be responsible for the waveform differences shown. A more careful look into these effects is planned.

The peak pressure level versus advancing-tip Mach number of two microphones is shown in Fig. 9, using the right-hand vertical

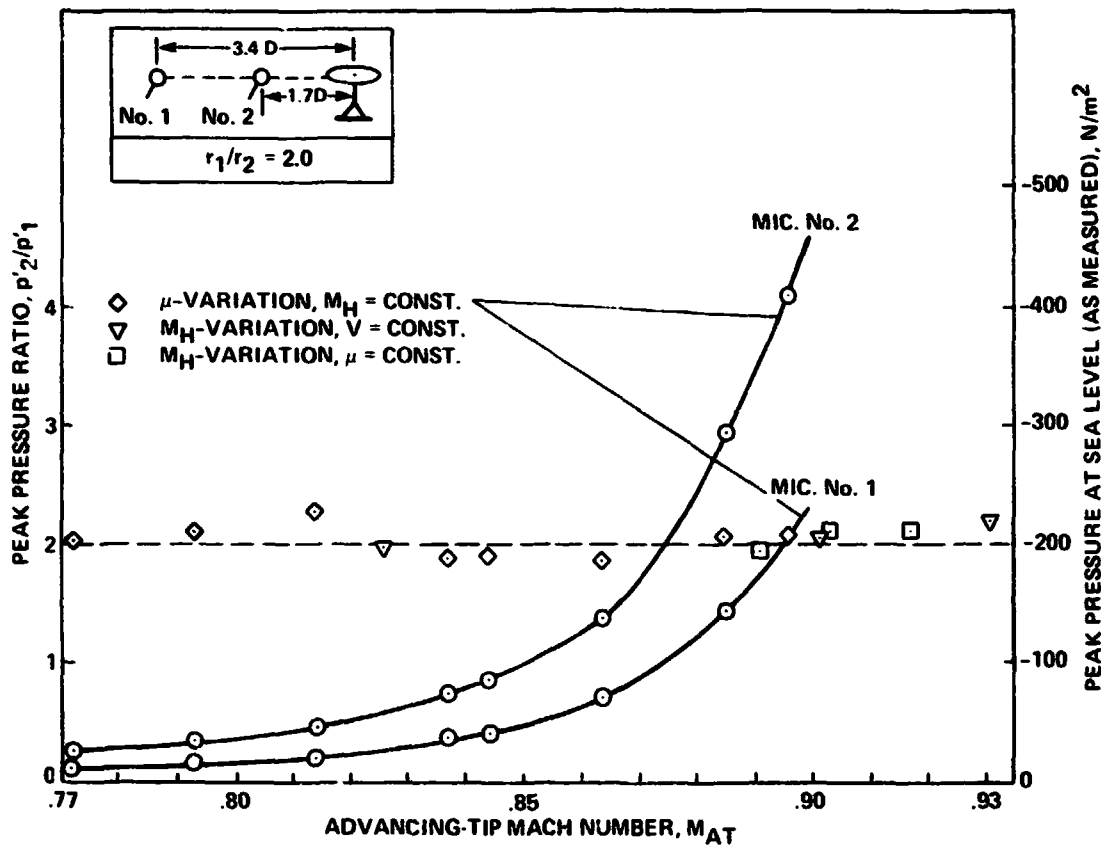


Fig. 9. Peak pressure decay rate for various operational conditions of the model rotor.

scale. The microphones are located along an imaginary line to the rotor hub directly ahead of the model rotor, the second microphone being exactly twice the distance from the hub as the first. The measured peak pressure ratio,  $P_2'/P_1'$ , is also plotted (using the left-hand scale) indicating a simple  $1/r$  decay law (spherical spreading) which is independent of advancing-tip Mach number. This figure shows that in-plane microphone locations greater than 3 radii from the rotor hub are in the high-speed impulsive noise acoustic far-field of the rotor. This result has been used in Figs. 7 and 8 to correct the model-rotor amplitudes for minor measurement-position differences between model-scale and full-scale rotor data. The result is also used in Fig. 10 to correct full-scale data to model-scale rotor non-dimensional distances. In some full-scale positions, these corrections were not insignificant.

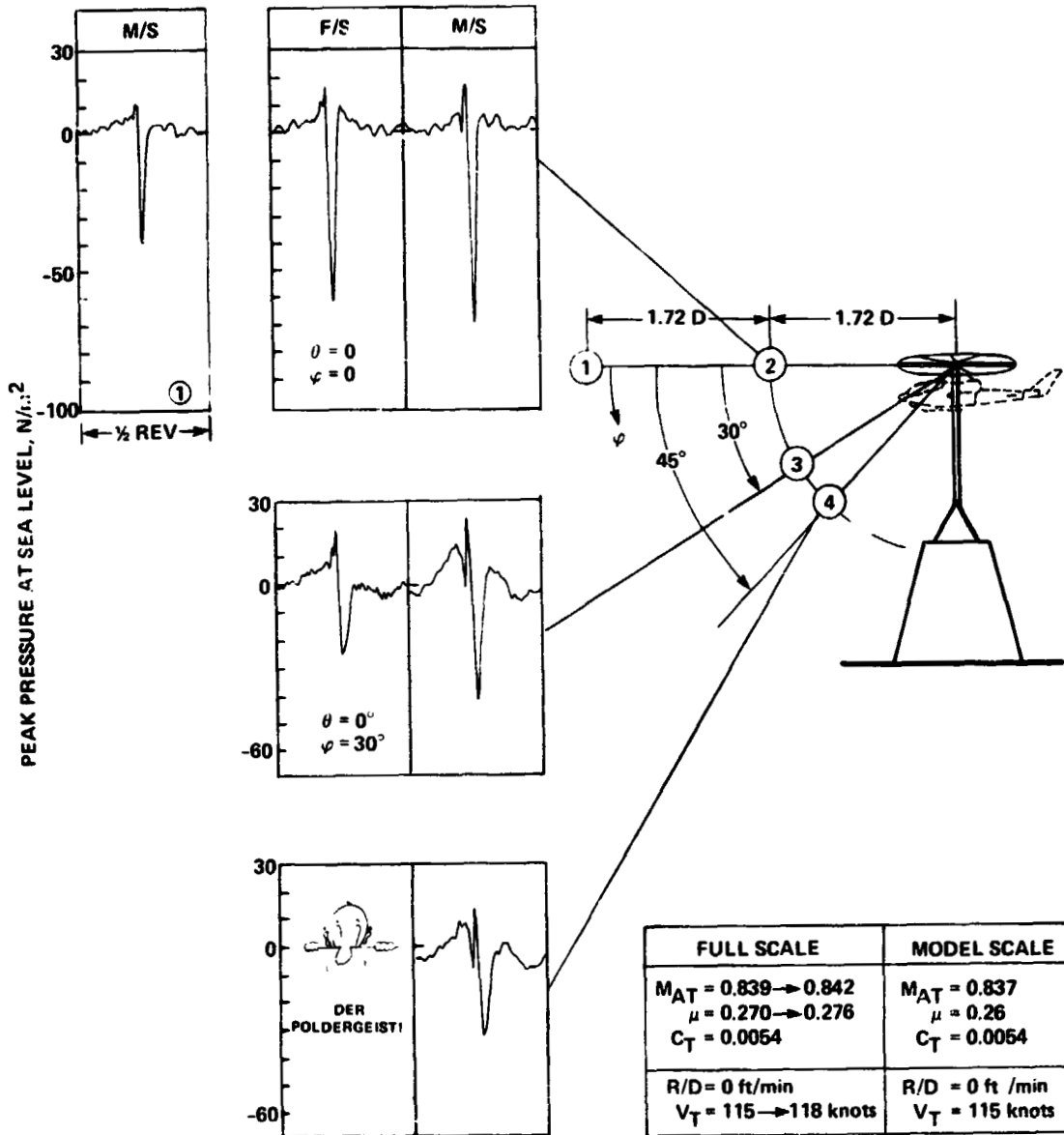
Directivity comparisons of model-scale and full-scale data are presented in the directivity profiles of high-speed impulsive noise shown in Fig. 10. The model-scale data shown in this figure were gathered under controlled conditions and can be considered to represent quantitative directivity profiles of radiated high-speed impulsive noise. However, the very nature of the in-flight, full-scale data-gathering technique makes similar measurements at other than a few carefully controlled microphone positions difficult at best. Measurement-position errors (azimuthal, elevation, and distance) and varying in-flight operating conditions tend to lessen the accuracy of the results. However, in spite of these qualifications, the comparisons illustrated in Fig. 10 are quite good, demonstrating the scalability of the high-speed impulsive noise.

Figure 10 presents the directivity of high-speed impulsive noise at an advancing-tip Mach number of 0.84 (below delocalization). The longitudinal directivity, shown in Fig. 10(a) is highly directional, as previously reported (Refs. [4], [8], and [10]). The peak negative amplitude of the nearly symmetrical pulse decreases rapidly at increasing longitudinal directivity angles ( $\phi$ ). The model-scale/full-scale comparisons suggest that the full-scale data shown at an estimated  $30^\circ$  below the horizontal might have been actually taken at slightly larger angles. Also shown in this figure is the microphone No. 1 waveform of the model-scale data taken at twice the distance of microphone No. 2. Although nearly identical in shape, it is approximately half the amplitude of the closer microphone, as would be predicted from the  $1/r$  sound decay law.

A lateral directivity comparison at this same advancing-tip Mach number is shown in Fig. 10(b). At the in-plane microphone positions, the model-scale/full-scale comparisons are excellent. At  $30^\circ$  under the rotor plane, the comparisons are only slightly degraded. Some of these waveform differences are attributable to the limited azimuthal locations where full-scale data are available. This figure confirms the focused nature of the high-speed impulsive noise. At this advancing-tip Mach number ( $M_{AT} = 0.84$ ) and advance ratio ( $\mu = 0.26$ ) the maximum noise intensity is directed forward but to the advancing side of the rotor. A similar longitudinal and lateral directivity comparison of high-speed impulsive noise at an advancing-tip Mach number of 0.895 (above delocalization) is given in Ref. [12]. As in the lower Mach number case presented here, the comparison between model-scale and full-scale is excellent.

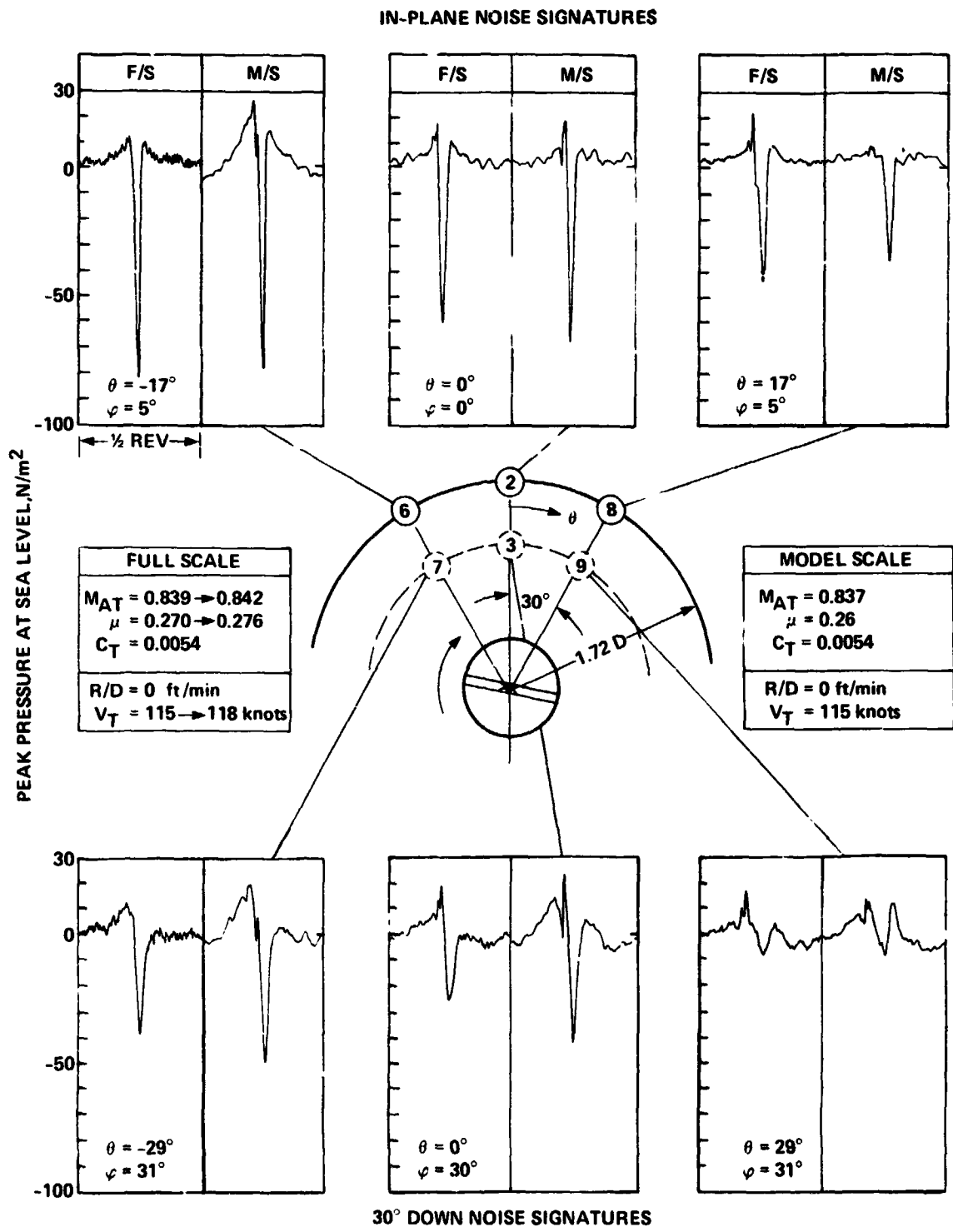
Taken together, Figs. 7-10 conclusively demonstrate that carefully designed and nondimensionally tested small-scale models can duplicate the high-speed impulsive noise generated by full-scale rotors. As demonstrated, the excellent aerodynamic and acoustic environment of the DNW makes it more than adequate for high-speed impulsive noise testing.

One of the major advantages of wind-tunnel testing over flight testing is that it makes it possible to explore wide ranges of test conditions in the relative safety and controlled conditions of the wind tunnel. Figure 11 presents high-speed impulsive noise levels and pulse shapes for in-plane microphone No. 2 over a range of



(a) Longitudinal directivity ( $M_{AT} = 0.837$ ).

Fig. 10. Comparison of model and full-scale impulsive noise directivity.



(b) Lateral directivity.

Fig. 10. Concluded.

ORIGINAL PAGE IS  
OF POOR QUALITY

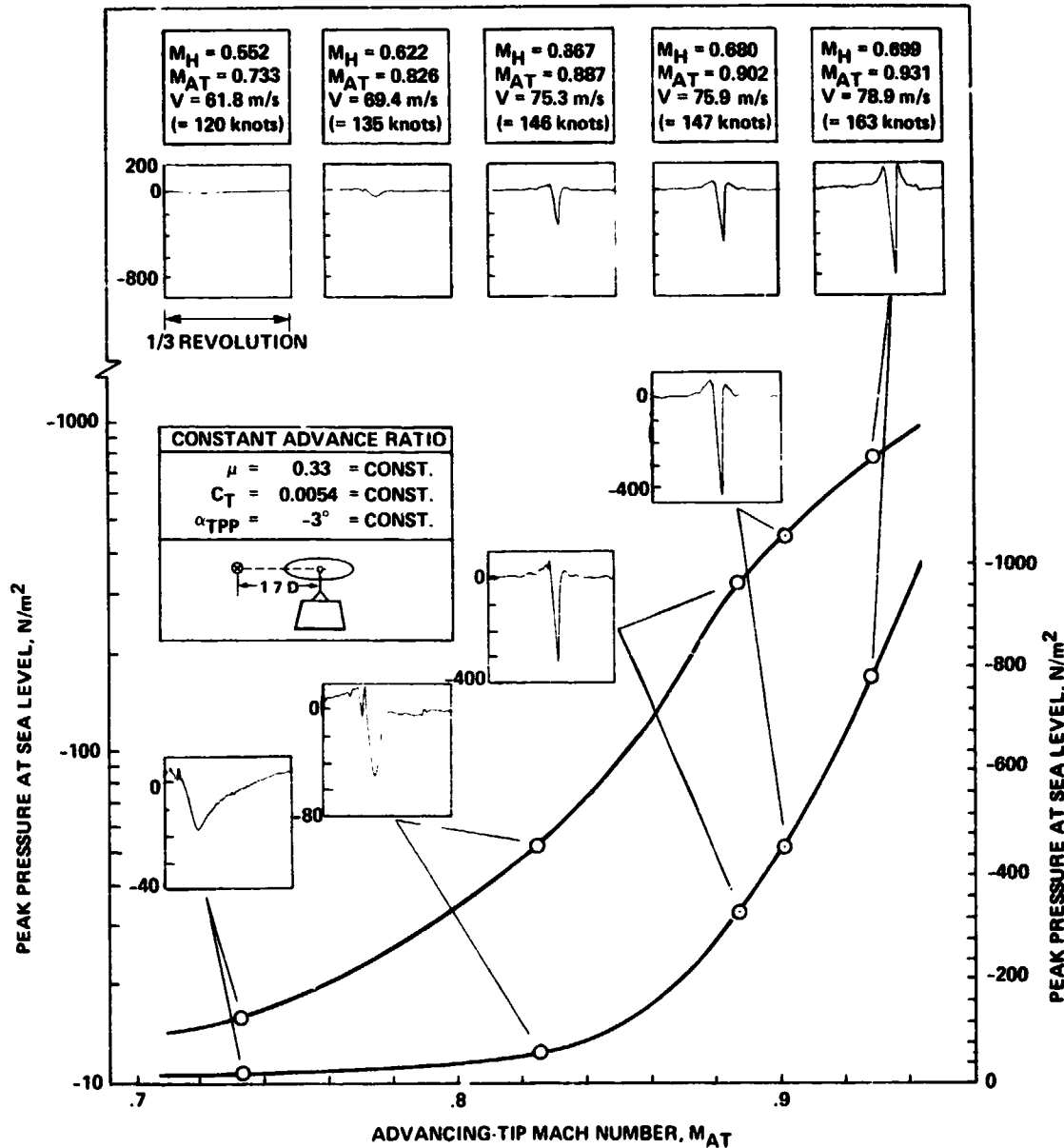


Fig. 11. High-speed impulsive noise versus advancing-tip Mach number at constant advance ratio (model scale).

advancing-tip Mach numbers from 0.73 to 0.93. For all of the cases shown in Fig. 11 the advance ratio  $\mu$  was held constant and the tunnel velocity and rotor rpm were varied accordingly. Large changes in peak pressure level and pulse shape are seen over a rather limited range of advancing-tip Mach numbers. As noted previously, delocalization occurs at an advancing-tip Mach number of about 0.89. These new measurements in the very favorable acoustical and aerodynamic environment of the DNW confirm the findings of Ref. [4], which show that advancing-tip Mach number is the key parameter of high-speed impulsive noise. In Fig. 11, the rate of increase of high-speed impulsive

noise level is plotted, using two scales: linear and logarithmic. The linear scale emphasizes the fact that the radiated noise increases to high levels with increasing advancing-tip Mach numbers. However, the logarithmic plot indicates that the rate of increase in level does not continue to increase. In fact, the logarithmic plot reaches its largest slope just before the delocalization advancing-tip Mach number ( $M_{AT} \approx 0.89$ ) and then begins to flatten out. A similar result was reported in Ref. [16] for a hovering rotor, where it was found that the local transonic flow field tended to weaken the rate of increase of acoustic levels at or above the hover delocalization Mach number. A similar mechanism is thought to apply here. However, the unsteadiness of the transonic aerodynamic field will undoubtedly influence the resulting acoustic radiation as well. Variations of the peak pressure levels and waveforms with the other scaling parameters (advance ratio, tip-path-plane angle, and thrust coefficient) were investigated during the DNW testing and are reported in Ref. [12]. Their influence on the radiated noise was confirmed to be less than that of advancing-tip Mach number.

## 6. Model-Scale Blade Pressures

Throughout the DNW testing, model rotor-blade pressure data were collected simultaneously with the rotor acoustics over the entire test envelope shown in Fig. 6. As previously mentioned, this envelope encompassed rotor operating conditions where both high-speed and blade-vortex interaction noise are known to occur. On-line monitoring of all the blade-pressure data indicated that it is of very high quality over the entire matrix of flight conditions. In keeping within the scope and purpose of this paper, selected blade pressures for two high-speed test conditions are presented that are of particular interest acoustically. The two conditions are those for which acoustic signatures were shown previously in Fig. 8. In that figure, model-rotor acoustic waveforms at tip Mach numbers of 0.864 and 0.896 were compared. The 0.864 Mach number condition exhibited a nearly symmetrical waveform, whereas the 0.896 acoustic waveform was characterized by a rapid (shock-like) pressure rise. The latter condition is slightly above the delocalization Mach number and the former (0.864) is, significantly for acoustics, below it. Since the blade pressures and acoustic data were acquired simultaneously in this test, the possibility of relating common characteristics in each was afforded. More specifically, an interesting aspect of the delocalization hypothesis is that there is a high subsonic Mach number where shock waves that exist on the rotor blade escape to the acoustic far-field. These waves are confined, however, to a region surrounding the rotor tip at Mach numbers only slightly below the delocalization Mach number but escape to the acoustic far-field at Mach numbers above it. In both cases, shock waves exist near the airfoil surface and, therefore, should be identifiable in the measured blade-pressure data.

Blade absolute pressures for the lower advancing-tip Mach number (0.864) are shown in Fig. 12 for one rotor revolution. The pressures are measured on the upper surface near the blade tip at 95.5% radius, are referenced to atmospheric pressure, and averaged

ORIGINAL PAGE IS  
OF POOR QUALITY

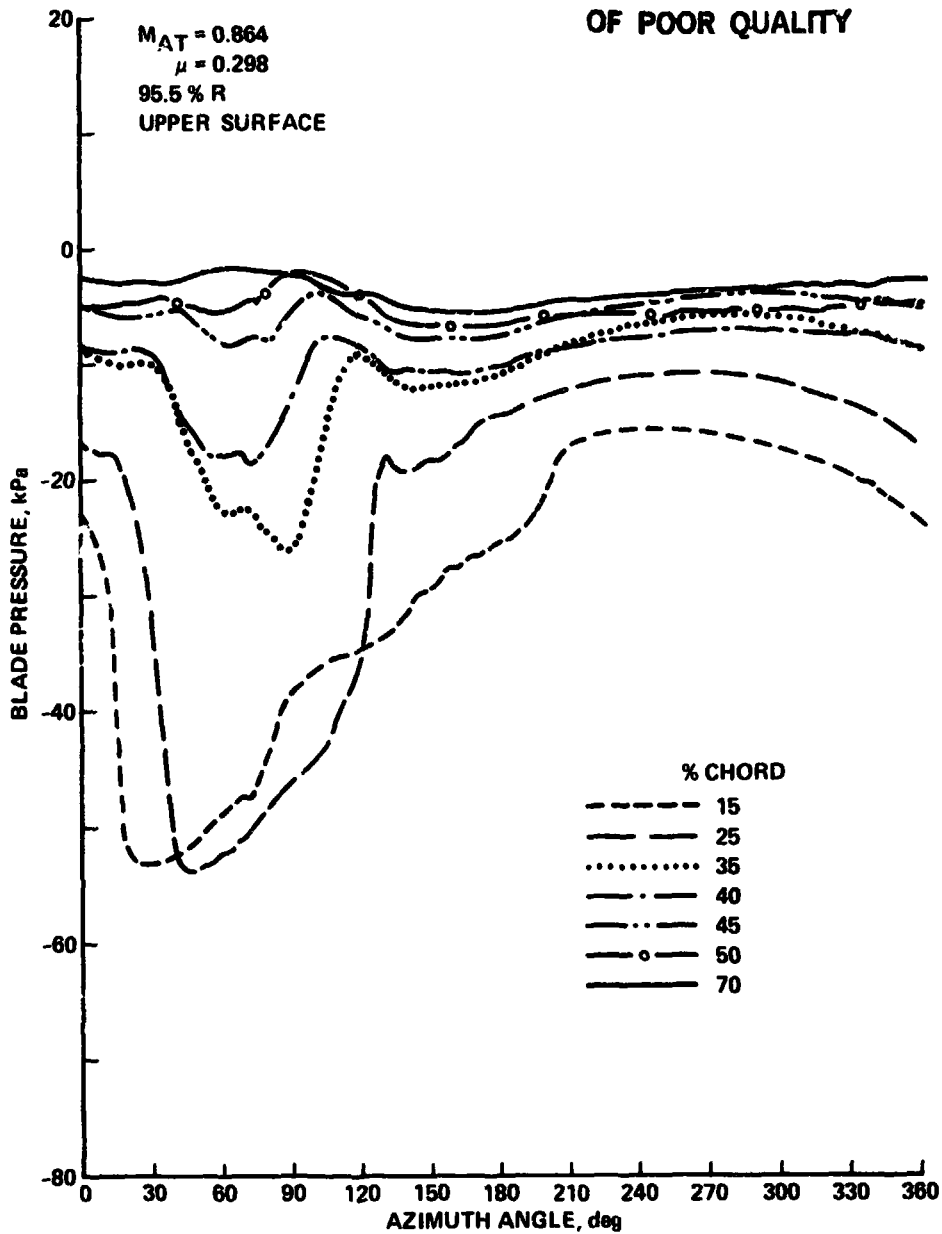


Fig. 12. Model OLS rotor upper-surface blade pressure versus azimuth for  $M_{AT} = 0.864$ , 95.5% R.

64 times. Pressure-time histories at chordwise locations from 15% to 70% chord are shown in the individual curves of the figure. Starting at  $0^\circ$  azimuth (blade pointing downstream) a large rapid decrease in pressure occurs near the leading edge (15% chord) and moves rearward on the blade (to 25% chord) as the blade advances to the  $45^\circ$  azimuth position. Beyond this point as the blade approaches  $90^\circ$ , there is a large drop in the negative pressure peak as indicated by the 35% chord transducer. This is characteristic of a shock formation between 25% and 35% chord at the  $90^\circ$  position. As the blade slows

ORIGINAL PAGE IS  
OF POOR QUALITY

$M_{AT} = 0.864$   
 $\mu = 0.298$   
95.5 % R  
UPPER SURFACE

from the maximum advancing-tip Mach number, the pressure discontinuity between 25% and 35% chord becomes stronger until the blade reaches  $120^\circ$  where there is a rapid collapse in pressure as the shock moves forward and past the 25% chord point. This same trend of shock formation and movement can be seen in Fig. 13 where blade-pressure coefficient  $C_p$  is plotted versus chordwise location at azimuthal angles from  $30^\circ$  to  $135^\circ$ . Again a strong upper-surface shock has been established between 25% and 35% chord at  $45^\circ$  azimuth. At  $90^\circ$ , the strength has decreased but grows again until the blade passes  $120^\circ$ . Both Figs. 12 and 13 indicate the formation of blade pressure discontinuities near the rotor-blade tip at an advancing-blade-tip Mach number of 0.864. Since the far-field acoustic waveform (Fig. 8) is nearly symmetrical, it would appear that this discontinuous blade-pressure disturbance is not preserved in the radiated acoustic signature.

In a similar manner, the upper-surface blade-pressure distribution at the

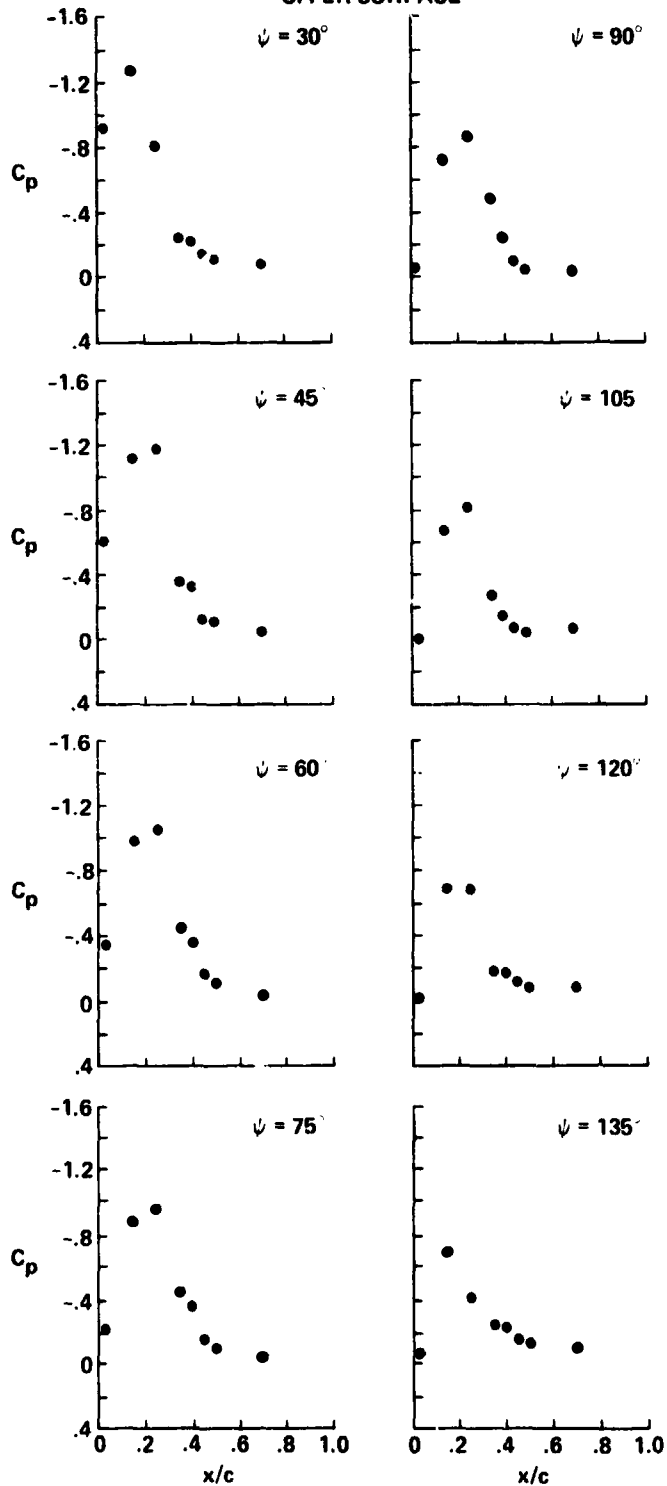


Fig. 13. Model OLS rotor upper-surface chordwise pressure coefficient versus azimuth for  $M_{AT} = 0.864$ , 95.5% R.

ORIGINAL PAGE IS  
OF POOR QUALITY

higher advancing-blade-tip Mach number (0.896) is presented in Figs. 14 and 15. Once again a large negative-pressure region is formed on the blade upper surface and moves rearward as the rotor blade approaches the 90° position. At this higher Mach number, however, the supersonic flow region extends farther back on the blade. Figure 14 shows that a large pressure discontinuity (rise) now occurs between 40% and 45% chord at the 90° position. As before, both Figs. 14 and 15 show that the shock remains on the airfoil during

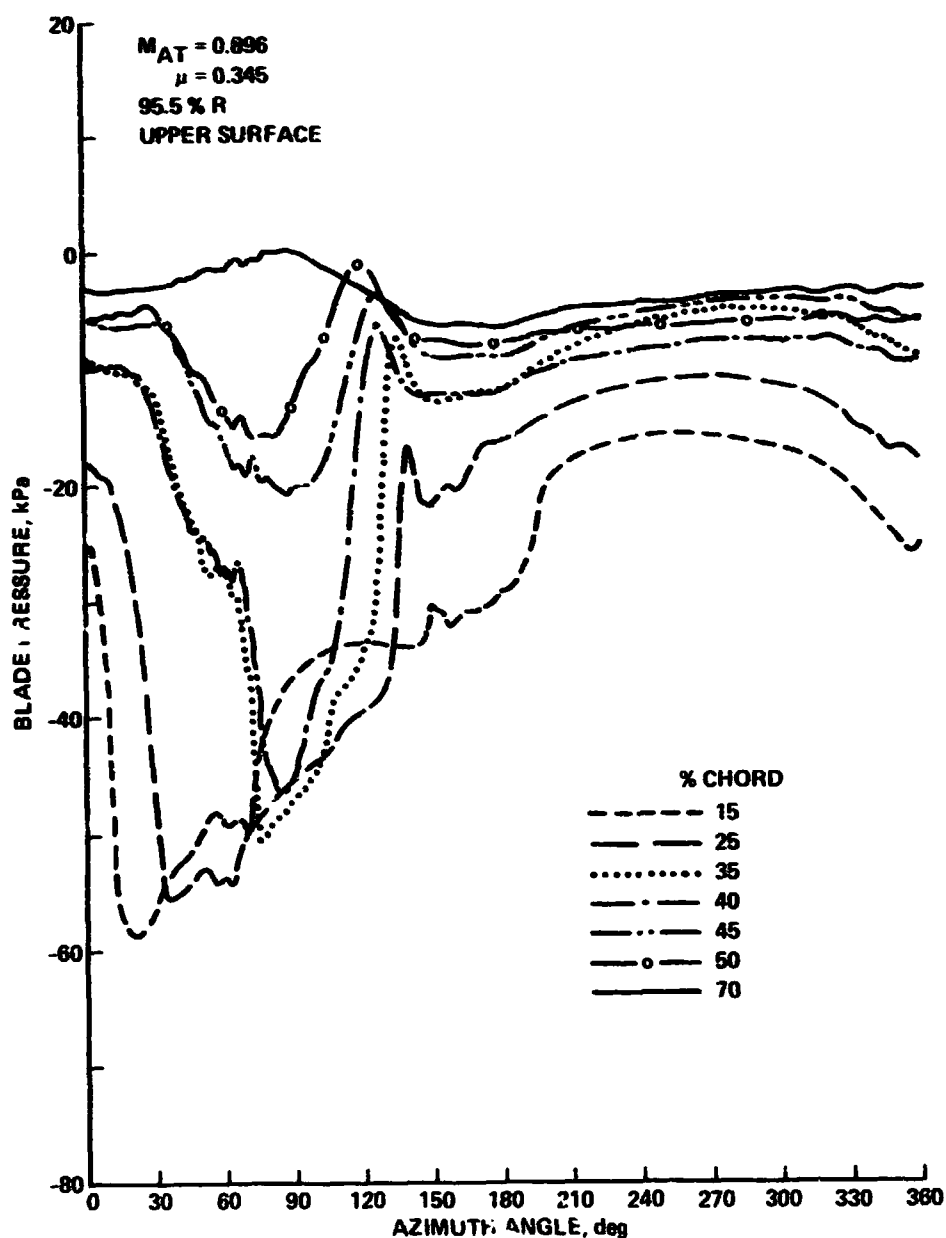


Fig. 14. Model OLS rotor upper-surface pressure versus azimuth for  $M_{AT} = 0.896$

$M_{AT} = 0.896$   
 $\mu = 0.345$   
95.5% R

UPPER SURFACE

deceleration past  $90^\circ$  until at  $125^\circ$  the shock has moved forward again and collapsed the large negative-pressure region. It should be noted that at this high-forward-speed condition, the tip-path-plane tilt was limited (as explained in an earlier section) so that the rotor is in a descent of 800 ft/min. The irregularities in the pressure distributions of Fig. 14 in the vicinity of  $60^\circ$  azimuth are believed to be the result of blade/wake interactions.

Unlike the lower Mach number case (0.864) in which strong discontinuities existed on the blade but not in the radiated acoustic signature, the advancing-tip Mach number case of 0.896 (Fig. 8) exhibits shock-like disturbances both on the blade and in the far-field acoustic waveform, indicating that above the delocalization Mach number the local shocks that exist near the rotor-blade surface radiate as shock waves to the acoustic far-field.

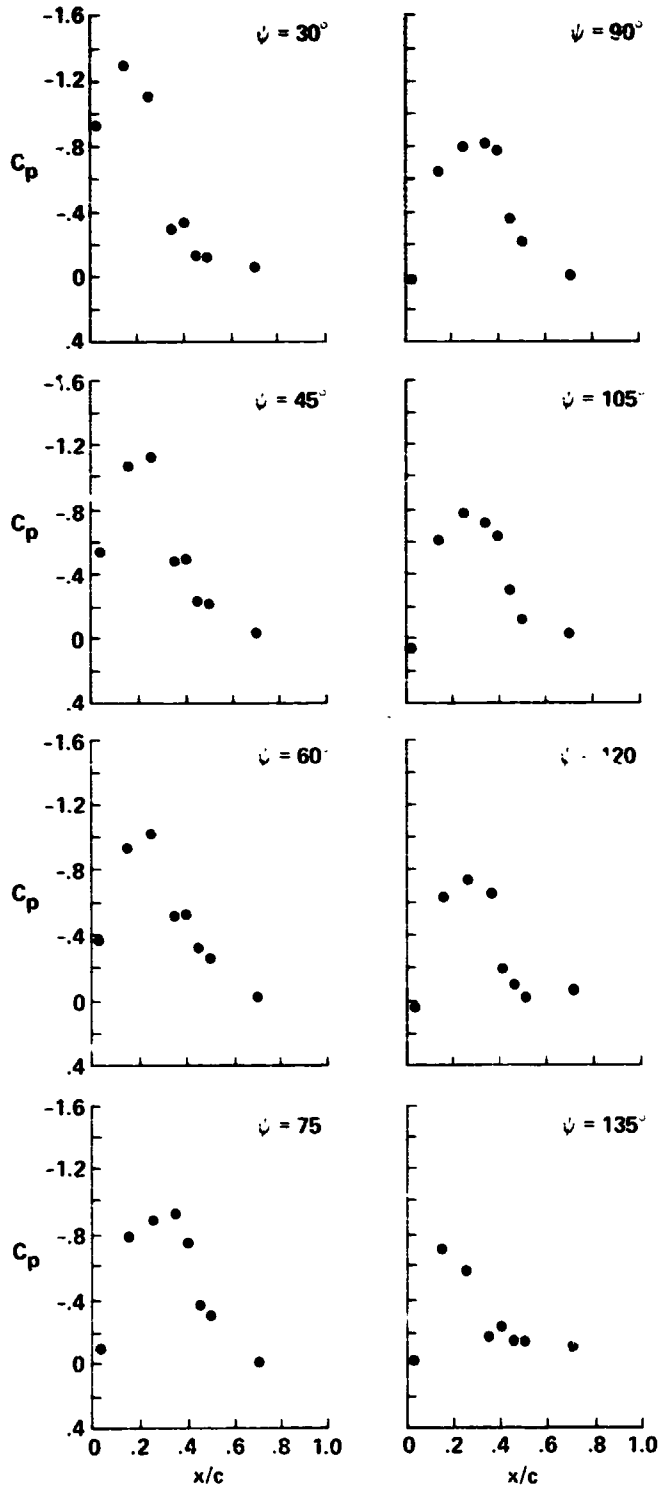


Fig. 15. Model OLS rotor upper-surface chordwise pressure coefficient versus azimuth for  $M_{AT} = 0.896$ , 95.5% R.

## 7. Concluding Remarks

Acoustic and blade-pressure data taken in the world's largest anechoic wind tunnel – the DNW in the Netherlands – have documented the high-speed noise radiated from a 1/7-scale model main rotor of the AH-1 series helicopter. The data confirm and expand many of the known features of high-speed impulsive noise. The major findings are as follows:

1) A set of nondimensional scaling equations was developed from the governing equations of rotor acoustics. These equations were successfully used to compare small-scale model rotor acoustic data taken at sea level in wind tunnels with full-scale acoustic data measured in-flight at altitude.

2) High-speed impulsive noise model-scale amplitudes and waveforms compare exceedingly well with full-scale in-flight acoustic data over a wide range of advancing-tip Mach numbers and directivity angles. These results conclusively demonstrate that model-scale rotors can be used to explore potential acoustic design changes on full-scale helicopters.

3) High-speed impulsive noise is a highly directional phenomenon – energy is radiated predominantly in-plane in the direction of forward flight toward the advancing-blade side of the rotor. Advancing-tip Mach number is the dominant nondimensional parameter that governs high-speed impulsive noise radiation.

4) Blade pressures show that local shock waves exist near the tip of the rotor blade and "delocalize" to the acoustic far-field above a "delocalization" advancing-tip Mach number. The mechanisms known to control delocalization for the hovering transonic rotor also appear to significantly influence the forward-flight transonic acoustic radiation. Unsteady transonic effects appear to exert a secondary influence on the acoustic radiation when compared with the effect of advancing-tip Mach number.

5) Microphones located at a distance of 3 radii from the rotor hub are in the acoustic far-field of high-speed impulsive noise. At greater distances, the peak negative pressure level decays according to a  $1/r$  law over the range of advancing-tip Mach numbers tested ( $M_{AT} = 0.7-0.94$ ).

6) For high-speed impulsive noise, signal-analysis techniques can be used to improve the signal-to-noise ratio of the in-flight data. By synchronizing with the large features of the impulsive waveform, in-flight acoustic data can be averaged. The resulting waveform does not contain bothersome tail-rotor periodic noise; it represents the amplitude and waveform from the main rotor only.

Perhaps the most important contribution of the present effort is the careful documentation of the high-speed impulsive noise waveforms. The quiet ambient and nearly anechoic properties of the DNW have minimized acoustic distortions. It is hoped that the high quality of the resulting data will be used to guide the development of

ORIGINAL PAGE IS  
OF POOR QUALITY

theory. The data can also be used to help interpret similar acoustic data under less ideal conditions.

Appendix: Scaling of Acoustic Pressures

The integral equation for the acoustic field generated by moving surfaces is given by (Ref. [15])

$$P'(x, t) = \frac{1}{4\pi} \left\{ \frac{\partial}{\partial t} \int_S \left[ \frac{\rho_o v_n}{r|1 - M_r|} \right]_{\tau} dS - \frac{\partial}{\partial x_i} \int_S \left[ \frac{P_{ij} n_j}{r|1 - M_r|} \right]_{\tau} dS + \frac{\partial^2}{\partial x_i \partial x_j} \int_V \left[ \frac{Q_{ij}}{r|1 - M_r|} \right]_{\tau} dV \right\} \quad (A1)$$

where

$$Q_{ij} = \rho u_i u_j + P_{ij} - a_{o0}^2 \delta_{ij}$$

and subscript o denotes ambient conditions. This equation contains three types of acoustic sources which are discussed in detail in Ref. [15]. The first is a "monopole" source, which is governed by the time-rate-of-change of fluid mass displaced by the moving surface; it is known to be a contributor to high-speed impulsive noise. The second term is a "dipole" source, which is dependent on a spatial derivative of local surface forces and is known to be an important contributor to blade-vortex interaction impulsive noise. The third term is a "quadrupole" source, which is governed by two spatial derivatives of the  $Q_{ij}$  stress tensor in the volume of fluid surrounding the blade.

To put Eq. (A1) in nondimensional form, define the following nondimensional parameters:

Nondimensional time:

$$\bar{t} = \frac{t}{2\pi/\Omega} \quad (\text{observer time})$$

$$\bar{\tau} = \frac{\tau}{2\pi/\Omega} \quad (\text{source time or retarded time})$$

Nondimensional geometry:

$$\bar{r} = \frac{r}{R}, \quad d\bar{S} = \frac{dS}{R^2}, \quad d\bar{V} = \frac{dV}{R^3}$$

Assuming that velocities normal to the rotor-blade surface,  $v_n$ , can be represented as

$$v_n = U \cdot \lambda$$

where  $\lambda$  = local surface slope, and remembering that

$$M = \frac{U}{a_0} \equiv \text{Mach number of the flow over the blade}$$

Defining  $M_T$  = rotational tip Mach number  $\equiv \Omega R/a_0$ ,

$$C_p'(\bar{x}, \bar{t}) = \frac{P'(\bar{x}, \bar{t})}{\rho_0 a_0^2}, \quad C_{p_{ij}} = \frac{P_{ij}}{\rho_0 U^2}$$

Equation (A1) becomes

$$\begin{aligned} \frac{P'(\bar{x}, \bar{t})}{\rho_0 a_0^2} \equiv C_p'(\bar{x}, \bar{t}) = & \frac{1}{4\pi} \left\{ \frac{M_T}{2\pi} \frac{\partial}{\partial \bar{t}} \int_{\bar{S}} \left[ \frac{M\lambda}{\bar{r}|1-M_T|} \right]_{\bar{t}} d\bar{S} \right. \\ & - \frac{\partial}{\partial \bar{x}_i} \int_{\bar{S}} \left[ \frac{C_{p_{ij}} n_j M^2}{\bar{r}|1-M_T|} \right]_{\bar{t}} d\bar{S} \\ & \left. + \frac{\partial^2}{\partial \bar{x}_i \partial \bar{x}_j} \int_{\bar{V}} \left[ \frac{C_{Q_{ij}}}{\bar{r}|1-M_T|} \right]_{\bar{t}} d\bar{V} \right\} \quad (A2) \end{aligned}$$

where

$$C_{Q_{ij}} = \frac{\rho}{\rho_0} m_i m_j + C_{p_{ij}} M^2 - \frac{\rho}{\rho_0} \delta_{ij}$$

$$m_i = \frac{u_i}{a_0}, \quad m_j = \frac{u_j}{a_0}$$

and

$$\bar{t} = \bar{t} + \frac{\bar{r}}{2\pi} M_T$$

Equation (A2) defines a nondimensional acoustic pressure coefficient at a measurement point in terms of nondimensional parameters. Given unique values of all the nondimensional parameters on the right-hand side of Eq. (A2), a unique value of  $C_p'(\bar{x}, \bar{t})$  is ensured. However, it should be noted that other governing nondimensional parameters are implicitly defined in this process.

Equation (A2) may be used to develop directly scaling procedures and rules for rotor testing. Consider two different sized but geometrically similar rotors of radius  $R$ , one full scale and a second,  $1/\gamma$  scale. We shall let

$$\gamma \equiv \text{scale factor} = \frac{R}{R_m}$$

**ORIGINAL PAGE IS  
OF POOR QUALITY**

where the subscript  $m$  denotes model scale. An important nondimensional parameter for acoustic scaling is rotational tip Mach number,  $M_T$ ,

$$M_T = \frac{\Omega R}{a_o} = \frac{\Omega_m R_m}{a_{o_m}}$$

To hold rotational tip Mach number the same for model and full scale, the rotational shaft rate must be adjusted so that

$$\Omega_m = \frac{R}{R_m} \frac{a_{o_m}}{a_o} \Omega = \gamma \frac{a_{o_m}}{a_o} \Omega \quad (A3)$$

Because nondimensional time must also be scaled,

$$t_m = \frac{1}{\gamma} \frac{a_o}{a_{o_m}} t \quad (A4)$$

In addition, Eq. (A2) requires that  $M$  be scaled. If we consider the tip of the rotor and neglect the spanwise flow along the blade, then

$$M = \frac{U}{a_o} = \frac{\Omega R + V \sin \psi}{a_o} = M_T (1 + \mu \sin \psi)$$

(A similar argument could be made at any blade radial station.) This implies that the advance ratio  $\mu$  must be scaled, that is,

$$\mu = \frac{V}{\Omega R} = \frac{V_m}{\Omega_m R_m} = \mu_m$$

Thus,

$$V_m = \frac{\Omega_m}{\Omega} \frac{R_m}{R} V = \frac{a_{o_m}}{a_o} V \quad (A5)$$

Equation (A2) also requires that  $C_{p_{ij}}$  and  $C_{Q_{ij}}$  be scaled for both model and full scale. This implies similarity in the aerodynamic flow field and scaling of rotor thrust along the blade at each azimuthal angle. This requirement is approximated by maintaining similar in-flow through the rotor disk by means of similar tip-path-plane angles and rotor-thrust coefficients.

The process of geometric scaling implies that all lengths are scaled by  $\gamma$ :

$$r = \gamma r_m \quad (A6)$$

In practical terms, this implies that model measurement microphones should be positioned  $\gamma$  times closer to the hub center than full-scale geometric distances.

#### Acknowledgments

In a test of this magnitude, there are many people who rightfully deserve recognition for a job well done. We offer our sincerest thanks to our friends and colleagues at the Army Aeromechanics Laboratory, NASA Ames Research Center; the Acoustics Department of the DFVLR, Braunschweig; the DNW Foundation and its parent organizations, DFVLR and NLR; NASA Ames Research Center; and the Army Structures Laboratory, NASA Langley Research Center.

#### References

- 1) F. H. Schmitz and Y. H. Yu, Transonic Rotor Noise – Theoretical and Experimental Comparisons, Vertica, Vol. 5, 1981, pp. 55-74.
- 2) M. P. Isom, Some Nonlinear Problems in Transonic Helicopter Acoustics, Poly M/AE Report No. 79-19, Polytechnic Institute of New York, Brooklyn, N.Y., May 1979.
- 3) D. Hawkings, Noise Generation by Transonic Open Rotors, Research Paper No. 599, Westland Helicopters Limited, Yeovil, England, June 22, 1979.
- 4) F. H. Schmitz, D. A. Boxwell, and C. R. Vause, High Speed Helicopter Impulsive Noise, Journal of the American Helicopter Society, Vol. 22, No. 4, Oct. 1977.
- 5) F. H. Schmitz and Y. H. Yu, Theoretical Modeling of High-Speed Helicopter Impulsive Noise, Journal of the American Helicopter Society, Vol. 24, No. 1, 1979.
- 6) H. Sternfeld, C. Bobo, D. Carmichael, T. Fukushima, and R. Spencer, An Investigation of Noise Generation on a Hovering Rotor, Part II, Report D210-10550-1, The Boeing Co., Vertol Div., Philadelphia, Penn., Nov. 1972.
- 7) H. Sternfeld and E. Schaeffer, An Investigation of Rotor Harmonic Noise by the Use of Small Scale Wind Tunnel Models, NASA CR-166338, 1982.
- 8) F. H. Schmitz and D. A. Boxwell, In-Flight Far-Field Measurement of Helicopter Impulsive Noise, Journal of the American Helicopter Society, Vol. 21, No. 4, Oct. 1976.
- 9) D. A. Boxwell and F. H. Schmitz, Full-Scale Measurements of Blade-Vortex Interaction Noise, Journal of the American Helicopter Society, Vol. 27, No. 4, Oct. 1982.

- 10) D. A. Boxwell and F. H. Schmitz, In-Flight Acoustic Comparison of the 540 and K747 Main Rotors for the AH-1S Helicopter, Appendix to U.S. Army Aviation Engineering Flight Activity Report 77-38, Edwards AFB, Calif., Oct. 1979.
- 11) F. H. Schmitz, D. A. Boxwell, S. Lewy, and C. Dahan, A Note on the General Scaling of Helicopter Blade-Vortex Interaction Noise, Presented at the 38th Annual National Forum of the American Helicopter Society, Anaheim, Calif., May 1982.
- 12) W. R. Spletstoesser, K. J. Schultz, F. H. Schmitz, and D. A. Boxwell, Model Rotor High-Speed Impulsive Noise - Parametric Variations and Full-Scale Comparisons, Presented at the 39th Annual National Forum of the American Helicopter Society, St. Louis, Mo., May 1983.
- 13) J. C. A. Van Ditsuizen, G. D. Courage, and R. Ross, Acoustic Capabilities of the German-Dutch Wind Tunnel, DNW, Paper No. 9.5, Presented at the 8th European Rotorcraft Forum, Aix-en-Provence, France, 1982.
- 14) G. A. Shockey, T. W. Williamson, and C. R. Cox, Helicopter Aerodynamics and Structural Loads Survey, Paper No. 1060, Presented at the 32nd Annual National Forum of the American Helicopter Society, May 1976.
- 15) J. E. Ffowcs-Williams and D. L. Hawkins, Sound Generation by Turbulence and Surfaces in Arbitrary Motion, Philosophical Transactions of the Royal Society of London, Series A, Vol. 264, 1969, pp. 321-342.
- 16) D. A. Boxwell, Y. H. Yu, and F. H. Schmitz, Hovering Impulsive Noise: Some Measured and Calculated Results, Vertica, Vol. 3, No. 1, 1979, pp. 35-45.